RES | THE SCHOOL for RENEWABLE ENERGY SCIENCE

The Effect of Ruthenium Crossover in Polymer Electrolyte Fuel Cells Operating with Platinum-Ruthenium Anode

Anna Trendewicz

---

eea grants
iceland liechtenstein norway

PROJEKT PL0460

UNIVERSITY OF ICELAND

University of Akureyri

The Effect of Ruthenium Crossover in Polymer Electrolyte Fuel Cells Operating with Platinum-Ruthenium Anode

Anna Trendewicz

A 30 ECTS credit units Master´s thesis

Supervisors

Piotr Zelenay, Ph.D., D.Sc. , Team Leader of Electrochemistry at Los Alamos National Laboratory, New Mexico, USA

Dr. David Dvorak, Professor at the University of Maine, Maine, USA

Dr. Thorsteinn I. Sigfusson, Professor at the University of Iceland and General Director of Innovation Center Iceland, Iceland

A Master´s thesis completed at

RES | The School for Renewable Energy Science

in affiliation with

University of Iceland &

University of Akureyri

Akureyri, February 2011

The Effect of Ruthenium Crossover in Polymer Electrolyte Fuel Cells Operating with Platinum-Ruthenium Anode

A 30 ECTS credit units Master´s thesis

RES | The School for Renewable Energy Science

Solborg at Nordurslod

IS600 Akureyri, Iceland

Telephone + 354 464 0100

www.res.is

The Master Thesis was supported by a grant from Iceland, Liechtenstein and Norway through the EEA Financial Mechanism - Project PL0460

Printed in February 2011

at Stell Printing in Akureyri, Iceland

ABSTRACT

Proton exchange membrane fuel cells with PtRu anode catalyst and Pt cathode suffer from severe performance degradation due to ruthenium dissolution from the anode, migration through Nafion® membrane, and deposition on the surface of cathode catalyst where it inhibits ORR. A detailed analysis of ruthenium crossover mechanism for a 5 cm^2 active area direct methanol fuel cell was performed to quantify the contamination rate and degree starting from contamination during manufacturing process, through initial humidification and ending with severe degradation due to operation. The change of ruthenium content on the cathode was defined with the use of CO stripping voltammetry and X-ray fluorescence. The fuel cell performance loss due to severe cathode contamination with ruthenium was measured to be 0.1 A/cm^2 at 0.5 V cell voltage for methanol-air operating mode. The air cathode performance loss was determined to be 80 mV. The ORR kinetics degradation was investigated by using platinum RDE contaminated with ruthenium via spontaneous deposition from 1.0 mM $RuCl_3$ in 0.1M $HClO_4$. The half-wave potential showed a negative shift by 20 mV just after 10 seconds deposition time. The CO stripping results obtained from RDE experiments show great similarity to results obtained from fuel cell tests. Initial anode cleaning was found out to greatly decrease the ruthenium contamination rate and thus enhance DMFC durability.

PREFACE

Thanks to their unique advantage of direct conversion of chemical energy into electricity, fuel cells have fascinated many excellent scientists worldwide over the last decades, not only chemists and chemical engineers but also mechanical engineers. They have invested effort in the development of this compact, silent and efficient technology which has tremendous potential to help satisfy world's ever growing energy demand.

Fuel cell performance is still not satisfactory and can be significantly improved. With the use of powerful electrochemical, mechanical and computational tools new tests are being developed every day to discover concealed properties of new catalytic materials and develop innovative solutions to existing technical problems and address challenges associated with the efficiency, durability, and cost of fuel cells.

This master's thesis is devoted to the development of low temperature proton exchange membrane fuel cells with particular interest in direct methanol fuel cells. It focuses on ruthenium crossover, which takes place when a platinum-ruthenium binary anode catalyst is used. The effect of this phenomenon is severe degradation of fuel cell performance which is one of the major barriers preventing commercialization of this energy-efficient and environmentally-friendly technology. If overcome, direct methanol fuel cells and reformate-operated fuel cells, which also use the PtRu catalyst at the anode (for CO tolerance), will be far more likely to become practically viable in portable power devices and stationary applications.

The goal of this research performed during four months of experimental work at Los Alamos National Laboratory was to provide better understanding of destructive contamination mechanism and contribute to the development of effective methods to mitigate the ruthenium crossover in fuel cells.

Acknowledgements

I would like to thank all the faculty members of The School for Renewable Energy Science for introducing me to renewable energy technologies and raising my interest in the fuel cell field.

I want to especially thank Piotr Zelenay, *Ph.D., D.Sc.*, who has led me through the mysterious world of fuel cells electrochemistry and greatly supported during my work with his advice.

I would also like to thank Christina M. Johnston, *Ph.D.*, Lior Elbaz, *Ph.D.* and other colleagues and friends in MPA-11 for their patience, commitment, advice and pleasant working atmosphere, which I found very helpful and supportive.

TABLE OF CONTENTS

LIST OF FIGURES

LIST OF TABLES

1 INTRODUCTION

Finding efficient, environmentally friendly and renewable energy sources is one of the biggest challenges for our civilization with its steadily increasing energy needs. It is crucial to find an alternative to depleting fossil fuel resources which are contributing to polluting the environment.

Fuel cells seem to assist with this problem by ensuring high efficiency due to direct conversion of chemical energy into electricity. Moreover, they demonstrate environmentally friendly performance with use of hydrogen or methanol as a fuel which can be both produced from renewable energy sources.

Among a variety of renewable fuels to be possibly used in fuel cells methanol seems to be the most convenient and easy to implement. Due to the high energy density, low cost, facile distribution and storage, methanol has distinctive advantages over hydrogen. Direct methanol fuel cells are a promising power source for portable devices, back-up power systems, and low-power vehicles, e.g., forklifts. In addition to having high specific energy and energy density ensuring longer operation times, one of the main advantages of the DMFC over the rechargeable batteries is that they do not require an external electrical power source for re-charge. The DMFC can be quickly re-fueled which is convenient and greatly enhances the mobility, enabling the use of electronic devices in remote areas where charging batteries is problematic.

The market for DMFCs for portable power applications such as notebook computers and mobile phones is expected to grow in the future according to [1]. However, DMFCs need to overcome several barriers before becoming commercially viable. The most significant barriers preventing large-scale commercialization are the following: the high cost of fuel cell components, the low rate of fuel oxidation and oxygen reduction reactions, methanol crossover, and fuel cell durability.

This work has focused on the investigation of catalyst degradation and thus cell performance degradation in low temperature proton exchange membrane fuel cells with binary platinum-ruthenium anode catalyst, supplied with methanol fuel. Interestingly, the platinum-ruthenium catalyst is also applied for PEM fuel cells operating on hydrogen fuel containing trace amounts of CO, i.e., hydrogen obtained from natural gas reforming. The required catalyst loading is significantly smaller in case of the reformate-operated fuel cells compared to DMFCs; however, the catalyst degradation mechanism shows great similarity. Thus, the results obtained in this work are likely to prove valuable for any fuel cells operating with a PtRu anode.

1.1 Methanol fuel

Methanol is the simplest of alcohols. Its chemical equation is CH_3OH. It is a toxic, colorless and tasteless liquid with a strong odor. It is known as "wood alcohol".

Methanol is produced mainly from natural gas. The production method consists of three major steps: syngas production, conversion of syngas into crude methanol, and methanol distillation. Natural gas is de-sulfurized and undergoes a steam reforming process to become syngas. The syngas is converted to methanol most commonly using the ICI Low Pressure Methanol (LPM) process in the presence of active cooper as a catalyst. Crude methanol is distilled in order to reach the required purity level. The benefit of using this production method is the relatively low production cost [2].

Another interesting feedstock for large-scale methanol production is coal. The production process used, Liquid Phase Methanol process (LPMOH), differs from processes used for natural gas feedstock. Firstly, coal is gasified to create syngas which is further processed in a slurry bubble column reactor (SBCR), where powdered catalyst is suspended in inert oil. The produced methanol has higher purity than the one created in LPM process, but it still requires a distillation process to obtain AA grade methanol. The LPMEOH process offers several advantages over traditional natural-gas-based processes which are the following: 5%-23% lower investment cost for the same methanol production capacity and 2%-3% lower operating costs due to 75% reduction in electricity consumption [2]. Another significant advantage of coal based methanol production is its compatibility with Integrated Gasification Combined Cycle (IGCC) for power generation. Methanol production from excess syngas in IGCC could lead to further production cost reduction.

Coal based methanol production would be an attractive opportunity for countries that have large coal resources to decrease their dependence on imported petroleum.

Methanol can be also produced from renewable energy sources such as wood, municipal solid waste (MSW), agricultural feedstock and sewage. The production method consists of gasification of wood, MSW or dried sewage to reach syngas which is further converted to methanol. Another possible production method is using landfill gas as a feedstock for and processing it with the same methods as those used for natural-gas-based methanol production. These production paths seem to be attractive and feasible. The dried sewage sludge gasification for methanol production is already being used in Berlin by one of Germany's water-supply and sewage-disposal company. This example proves feasibility of commercial methanol production from waste water treatment plants.

Methanol is already commonly used as a vehicle fuel. Most of such vehicles operate with an internal combustion engine which uses a mixture of 85% methanol and 15% of unleaded gasoline. Pure methanol can be used as a substitute for diesel fuel and as a fuel for fuel cell vehicles [3]. The implementation of refueling infrastructure for methanol is much easier than for hydrogen due to convenient transportation and storage of a liquid fuel. Moreover, methanol safety codes and standards are similar to those of gasoline, whereas pressurized or liquefied hydrogen storage procedures are much more complex. The use of methanol fuel, especially when produced from renewable energy sources, is a

simple way to achieve significant greenhouse gases emissions reduction from transportation.

Methanol is also an attractive fuel for portable power. The main advantages over hydrogen are the following: high energy density, convenient storage in a liquid without the need for pressurization and direct use of methanol fuel which eliminates the need of complex reforming devices, thus decreasing the mass and volume of the system. The main advantage of the DMFC over batteries is high mobility and the avoidance of time consuming electrical charging which is restricted by electricity availability.

1.2 Perspectives for methanol fuel and DMFC use in Poland

Poland has large coal resources which are used mainly in power plants for electricity production. This use has low efficiency and contributes to huge CO_2 and other greenhouse gases emissions. However, Polish coal could be exploited in a more efficient and environmentally-friendly way. It is an attractive feedstock for IGCC for power generation and methanol production from excess syngas.

There are already plans being made in this direction by a chemical plant in Kędzierzyn, the city which is investing 1.25 bln Euro in a coal gasification plant [4]. This investment will cause a decrease in CO_2 emissions and serve as a gas source allowing the plant to become independent of the natural gas supply from Russia. The investment will also contribute to lowering of the plant production cost as coal-based syngas is less expensive than the natural-gas-based syngas the plant is currently using. The coal gasification plant will use excess syngas for methanol production and will be capable of delivering 0.5 mln tons of methanol per year. This would be enough to supply current methanol demand and eliminate the need for methanol imports.

Poland has a large potential for low cost methanol generation which could be exported or used domestically. Methanol could be used as transportation fuel thus decreasing dependence on imported petroleum and, if produced from biomass or other renewable energy resources, decrease Polish GHG emissions from the transportation sector. During the transition, methanol could be used to fuel conventional vehicles with ICE; in the long term, fuel cell vehicles could be introduced. Methanol could be also used to supply portable power devices if they become commercially available in Poland in the future.

Fuel cell research and development of fuel cell technology in Poland is performed by scientific organizations such as Polish Hydrogen and Fuel Cell Association and Polish Hydrogen and Fuel Cell Technology Platform. The main goals of these organizations are the following: promotion and development of fuel cell technology, supporting R&D initiatives, education, and stimulating interest in hydrogen and fuel cells. These organizations are active participants in European conferences and organize summer schools [4].

2 DMFC PERFORMANCE

2.1 Electrochemistry

The direct methanol fuel cell is an electrochemical device which converts chemical energy of liquid methanol to electricity. The schematic diagram of a DMFC fuel cell depicting its operating principle is shown in Figure 1. A typical fuel cell consists of a membrane-electrode assembly (MEA), gas diffusion layers (GDLs) for both anode and cathode sides, and bipolar plates with machined flow fields. Membranes used in DMFCs are usually made of Nafion® (a perflurosulfonic acid polymer made by DuPont) and their functions are to conduct protons from the anode to the cathode side and to separate the fuel and oxidant. The anode and cathode catalyst layers' primary function is to increase the reaction rates of the fuel and oxidant. Gas diffusion layers supply reactants to catalyst layers and remove products. They usually consist of a backing layer which is made of carbon cloth or carbon paper and a microporous layer (MPL) which is made of hydrophobic polymer and carbon powder.

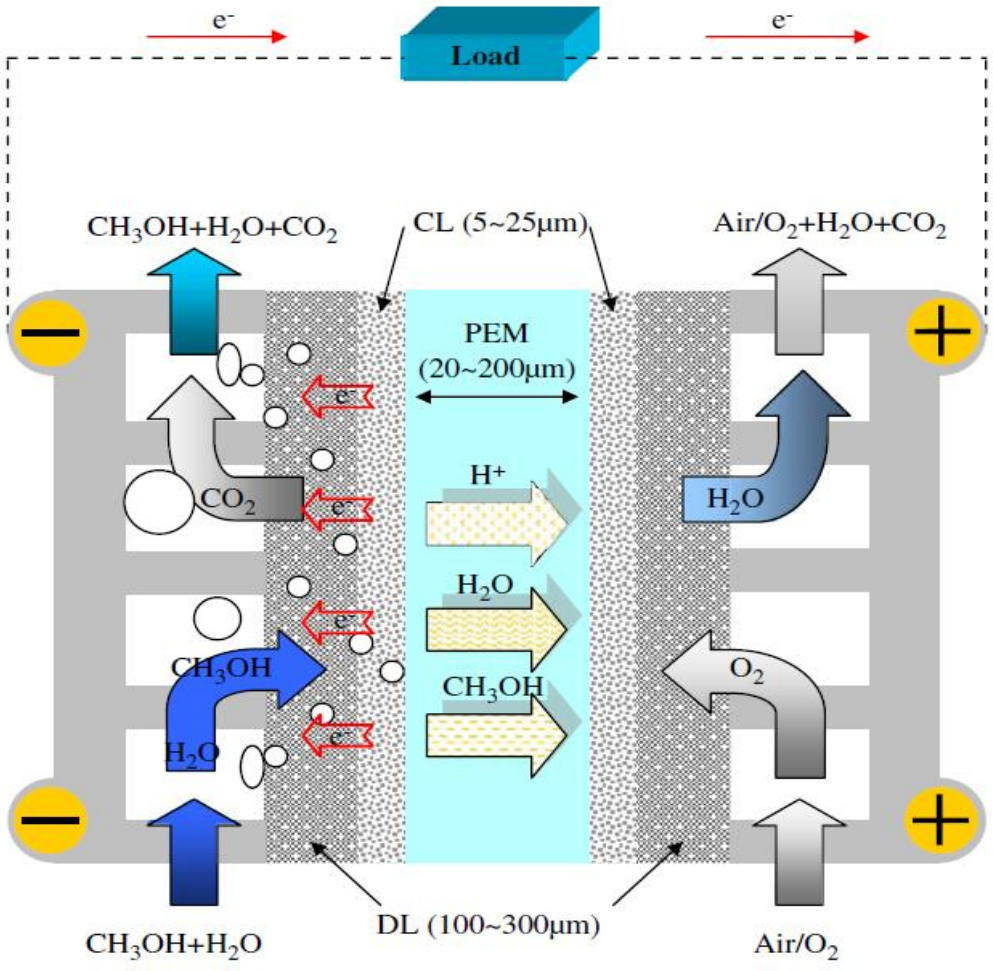

Figure 1. DMFC and PEM fuel cell [5].

Methanol is oxidized at the anode according to the following reaction (Equation 1).

$$CH_3OH + H_2O \longrightarrow CO_2 + 6H^+ + 6e^- \quad (1)$$

The products of the reaction are CO_2, six protons, and six electrons per every methanol molecule. The electrons are transferred through an external circuit, protons are transported through the membrane, and CO_2 is removed from the anode together with excess methanol and water. The reversible potential of methanol oxidation reaction is *ca.* 0.02 V versus standard hydrogen electrode [6].

Methanol fuel is supplied as a liquid solution and the product of the oxidation reaction is gaseous CO_2. The anodic side of the MEA needs to be different from the one used for hydrogen fuel. The gas diffusion layer needs to contain hydrophilic and hydrophobic pores. Hydrophilic pores ensure transport of methanol to the reaction zone, whereas hydrophobic pores ensure CO_2 removal. The appropriate ratio of hydrophobic to hydrophilic pores is obtained by addition of Nafion® and PTFE to the GDL.

The methanol oxidation reaction is sluggish because of CO formation as an intermediate product of methanol oxidation. CO adsorbs strongly on platinum sites, preventing further methanol adsorption and its initial dehydrogenation. In order to enhance the methanol oxidation rate, high loading platinum-ruthenium catalyst is used. Ruthenium is known to preferentially oxidize CO at potentials lower than in the case of platinum. The optimum Pt-to-Ru ratio, when CO oxidation occurs at the lowest possible potential, was experimentally determined in [7] and was found to be 46 wt % Ru.

The methanol solution needs to be supplied in excess to the anode catalyst in order to achieve uniform reactant distribution across the MEA surface and avoid performance losses due to mass transport limitations.

The oxygen is reduced at the cathode according to reaction (Equation 2) with the reversible potential of 1.23 V versus standard hydrogen electrode.

$$1.5\ O_2 + 6\ H^+ + 6\ e^- \longrightarrow 3\ H_2O \quad (2)$$

The oxygen reduction reaction is well known to be slow. In order to reduce one mole of oxygen, four electrons are needed and kinetics limits the reaction rate. In direct methanol fuel cells the reaction rate is further lowered by methanol migration (crossover) through the membrane and its oxidation at the cathode. In order to enhance oxygen reduction reaction (ORR) rate and achieve acceptable performance platinum catalysts are used at the oxygen cathode at loadings significantly higher than those used in hydrogen fuel cells.

The overall direct methanol fuel cell reaction is given by Equation 3.

$$CH_3OH + 1.5\ O_2 \longrightarrow CO_2 + 2\ H_2O \quad (3)$$

Theoretical cell voltage, according to this reaction is equal to 1.21 V at 25°C. However, experimentally achievable open cell voltage (OCV) is usually about 0.8 V due to irreversible losses caused by high overpotential of anode and cathode reactions (including that resulting from methanol crossover).

2.2 Methanol crossover

One of the biggest challenges of operating on methanol fuel is the permeation of methanol by diffusion and, to a much lesser degree, by electro-osmotic drag through the membrane. This phenomenon has basically two negative effects on the fuel cell performance. First, the fuel that crosses the membrane is not oxidized at the anode and contributes to lower fuel efficiency. Second, methanol is oxidized at the cathode thus inhibiting oxygen reduction reaction and decreasing cathode potential (mixed methanol oxidation and oxygen reduction potential) which contributes to a decrease of cell voltage.

Methanol oxidation at the fuel cell cathode results in electron generation and is observed in current density commonly defined as crossover current density ($j_{crossover}$). This parameter is easy to measure and serves as a tool for quantifying the flux of methanol molecules across the membrane. The experimental way to measure crossover current density is to supply the anode with methanol and the cathode with nitrogen, provide an external potential source for voltage sweeping and to record the current density.

Methanol crossover is driven by concentration gradient between the anode and the cathode side, so the rate of mass transport increases as methanol fuel concentration increases. The methanol crossover is most significant at low current densities. Under high current density operating conditions a large fraction of methanol is consumed at the anode, which causes the concentration gradient between the anode and the cathode to decrease. Using more concentrated methanol solution enables achieving higher current densities and thus higher power densities; however at low current densities the fuel is not efficiently consumed because of the large rate of methanol crossover [6].

Addressing methanol crossover challenges involves balancing trade-offs, i.e., methanol crossover increases with temperature increase, but so does reaction kinetics, the effect that more than offsets the crossover rate increase. [8]. Another example is that methanol crossover increases with membrane thickness reduction; however thickness reduction has also a positive effect of decreasing the ionic resistance.

Various designs have been tested to lower methanol crossover and allow anode operation at high methanol concentration. One such design concept includes an anode catalyst layer in the form of a catalyzed diffusion medium (CDM) which acts as a methanol diffusion barrier. It can operate in combination with a highly hydrophobic cathode microporous layer (MPL). The MPL increases water pressure and induces water flow from the cathode to the anode, thus offsetting cathode flooding [9].

3 DMFC DEGRADATION MECHANISMS

Direct methanol fuel cell performance deteriorates with time. As the cell voltage decreases in time, the required current to maintain constant power has to increase. Finally, the voltage degradation becomes so large that it is impossible to maintain required power as the necessary current density can no longer be achieved.

The effect of voltage loss on required current density to provide required-power is illustrated in Figure 2.

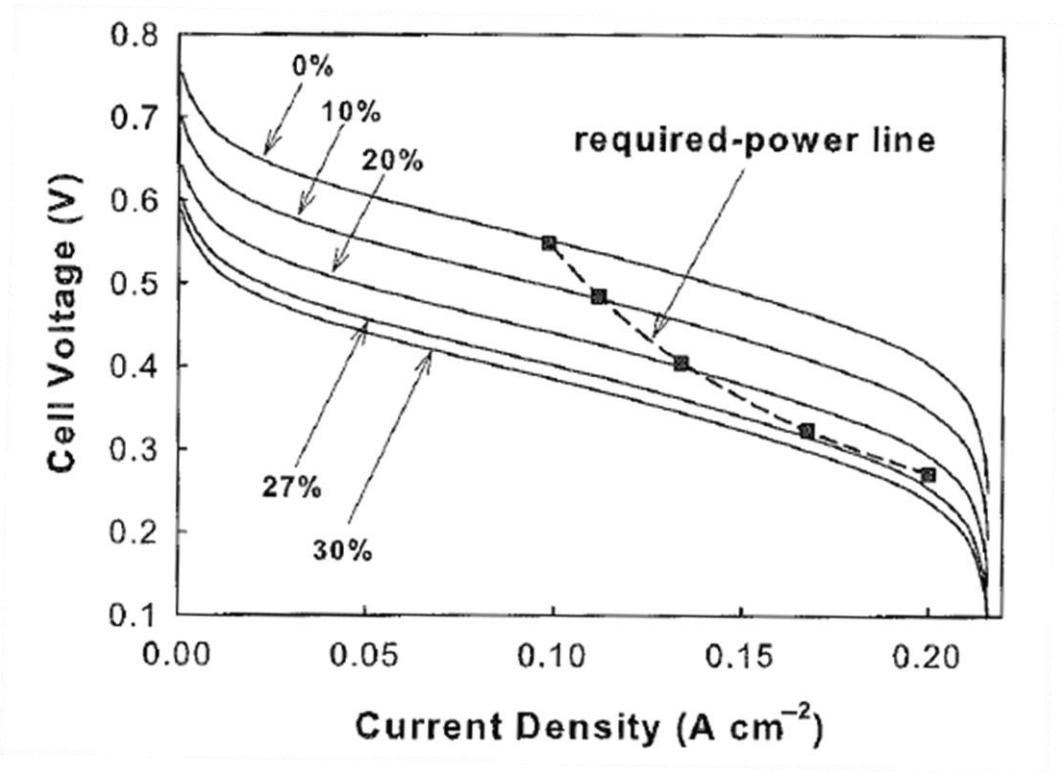

Figure 2. Influence of performance loss on fuel cell operation point [10].

The performance losses that occur during cell operation are of dual nature: recoverable and unrecoverable losses. Recoverable losses include the following: cathode catalyst surface oxidation, cell dehydration, and incomplete water removal from the catalyst layer or GDL. They can be reversed partially or even fully by restarting a fuel cell or applying appropriate reversal measures i.e. catalyst reduction by polarization or lowering the humidification level. Unrecoverable losses include the following: loss of electrochemical surface area of catalysts, ruthenium crossover, and membrane degradation. They cannot be reversed during cell operation. The unrecoverable performance losses are mostly related to catalyst degradation or membrane-electrode interface degradation.

3.1 Membrane-electrode interface degradation

The main causes of membrane-electrode interface degradation are differences in physicochemical properties of membrane and electrode, the use of elevated temperatures, and high flux of charged particles. The degradation usually occurs at the anode-membrane interface and is typically bigger when non-Nafion® membranes are used because of poor compatibility between the non-Nafion® membrane and Nafion®-containing electrode. The compatibility is reflected by the interfacial resistance value. Usually systems show stable performance when the initial interfacial resistance is below 20 $m\Omega cm^2$ [10].

An additional cause of membrane-electrode interfacial degradation during fuel cell operation can originate from the difference between the dimensional change of membrane and the electrode due to hydration. This causes a mechanical stress which may lead to local MEA delamination that tends to expand in time. In order to enhance wetting properties between membrane and electrode the following processes are used: electrophoretic processing, whereby carbon particles and Nafion® ionomer are deposited on PEM along a potential gradient, plasma treatment, whereby plasma activation is used, and wet-glue processing, whereby a Nafion® precursor is used between membrane and electrode to improve binding [10].

3.2 Catalyst degradation

3.2.1 Surface oxide formation

DMFCs suffer from high anode overpotential. At high cell operating voltage the cathode potential is at least 0.8-0.9 V versus the hydrogen reference electrode [10], which favors the formation of oxides and hydroxides on the platinum catalyst surface, thereby contributing to the reduction in catalyst activity and decrease in ORR rate due to the blocking of catalyst active sites. The oxides layer is typically formed within the first two hours of DMFC operation. The oxides continue to restructure, however, which causes changes in electronic properties of catalyst and further reduction in the ORR rate.

Performance degradation by surface oxides formation is recoverable by surface reduction. It can be done by using an air-break method, where air supply is cut off while maintaining the power. The remaining cathode oxygen is gradually used up, ultimately resulting in the reduction of oxides.

3.2.2 Loss of electrochemically active area

Another catalyst degradation mechanism is the loss of active electrochemical surface area due to cathode and anode catalyst particle sintering. There are three mechanisms of this loss: dissolution, migration of particles, and carbon corrosion. However, the loss of electrochemically-active surface is partly compensated by specific DMFC properties such as the increased specific activity of larger catalyst particles, lower sensitivity to surface

area loss due to high catalyst loading and re-deposition of platinum on the surface of nanoparticles, which decreases the rate of the active area loss [10].

3.2.3 Ruthenium crossover

Ruthenium-platinum catalyst is the most active and commonly used in electrochemical methanol oxidation. However, PtRu catalyst is thermodynamically unstable under the operating conditions of the DMFC anode. As a result, ruthenium tends to leach from the anode catalyst and migrates across the membrane from the anode to the cathode, deposits on the cathode catalyst, eventually inhibiting the ORR. There are two hypothetical causes of ruthenium migration (crossover): (1) instability of Ru in the PtRu alloy or elemental ruthenium under cell operating conditions and (2) mobility of ruthenium oxides present in anode catalyst. In addition to decreasing ORR rate, the presence of ruthenium at the cathode contributes to increased rate of surface oxide formation. The total unrecoverable loss due to the presence of Ru at the cathode has been reported to be in a range of 40-200 mV [10].

Ruthenium crossover can be recorded and quantified using CV, CO stripping, X-ray diffraction and X-ray fluorescence. CV enables the study of changes in the cathode's double-layer capacitance, observation of the changes in oxide reduction peak size and measurement of electrochemically-active area [11]. The carbon monoxide stripping technique provides information about electro-active surface area and qualitative information about changes in the ruthenium content. X-ray diffraction characterizes crystal structure, phase purity, and particle size, whereas X-ray fluorescence provides information about chemical composition and mass fraction of particular elements.

There are two mechanisms of ruthenium crossover: current-less and current-assisted. The current-less crossover is visible from the negative shift of CO stripping peak after humidification, even before operation. It includes the contamination resulting from MEA manufacturing.

The methods to limit the phenomenon of current-less ruthenium crossover in DMFC's include the following: high temperature cure of the anode catalyst by hot-pressing, pre-leach of ruthenium catalyst in aqueous solution of inorganic acid, use of low permeability membranes and electrochemical removal of mobile ruthenium. Current-less ruthenium contamination can be partially recovered by cycling cathode potential between 0.1 and 1.3 V according to [11].

The current-assisted crossover occurs under fuel cell operating conditions and is visible as a negative shift of CO stripping peak and shape differences. It was discovered that the cathode contamination rate significantly accelerates when the anode is operated at high potentials such as 0.95 V-1.3 V. Contrary to current-less contamination, a significant current-assisted contamination of the cathode, cannot be reversed by potential cycling [11]. The results of research carried out at Los Alamos National Laboratory on the effect of current-assisted cathode contamination on cell performance, presented in details in [11], are summarized in Figure 3.

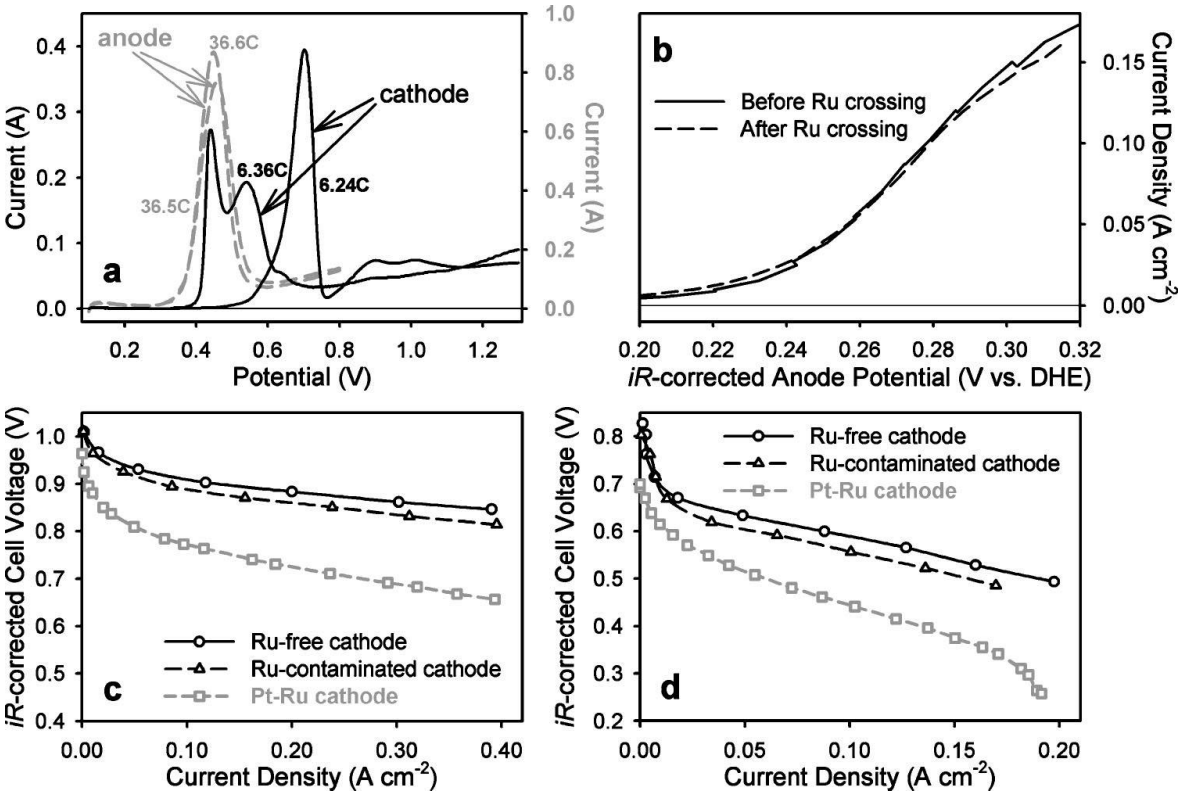

Figure 3.Effect of ruthenium contamination on DMFC performance [11].

Ruthenium contamination of cathode was reported not to affect the electrochemically active surface area of either the anode or the cathode catalyst (Figure 3a). The anode catalyst activity for methanol oxidation remained constant as well (Figure 3b). However, a significant loss of performance can be seen in polarization curves for hydrogen fuel (Figure 3c) and methanol fuel (Figure 3d). The voltage drop was reported to be 25 mV and 40 mV for hydrogen and methanol operating modes, respectively.

The ruthenium crossover phenomenon is not limited to direct methanol fuel cells. It also occurs in polymer electrolyte fuel cells operating on hydrogen reformate, as briefly mentioned in Chapter 1. Hydrogen gas produced by steam reforming or partial oxidation of hydrocarbons usually contains 10-50 ppm of CO and 20-25% of CO_2 [12]. The presence of CO, which is poisonous to Pt catalyst, forces the use of PtRu catalyst for the anode.

Fuel cells with a PtRu anode catalyst operating on reformate show performance degradation after AST cycling test according to [13]. Polarization curves at the beginning of life and after 2500 AST cycles for different relative humidity are shown in Figure 4.

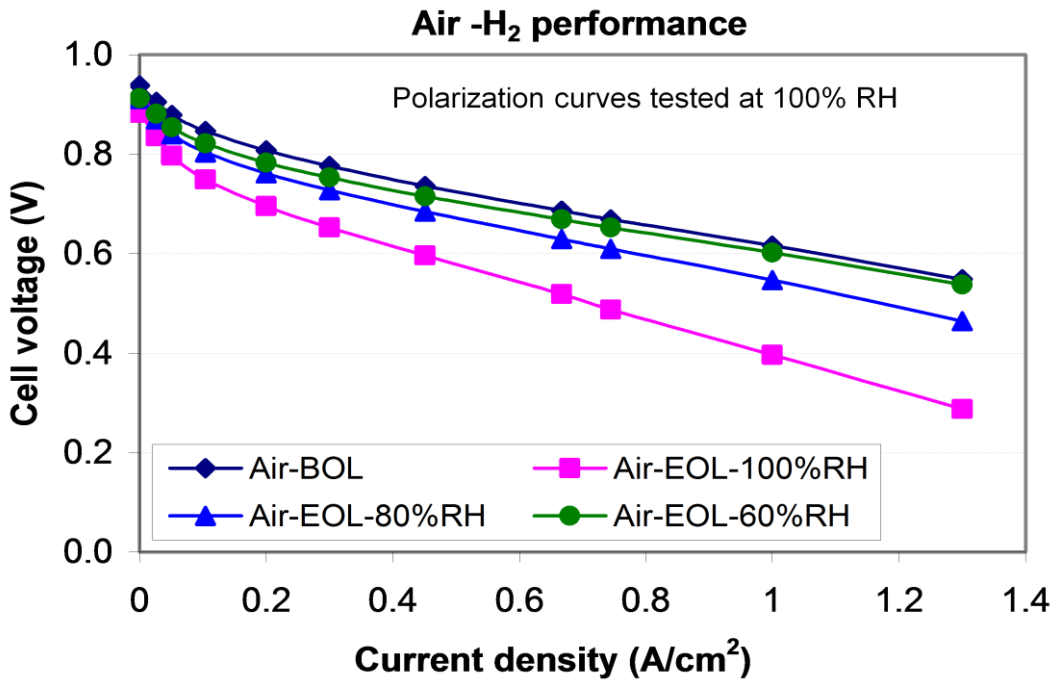

Figure 4. Polarization curves after AST cycling test for different relative humidity.[13]

It is clear that performance loss is more severe when relative humidity is higher. The loss is assigned to ruthenium deposition on the cathode. CO stripping experiments clearly indicate the presence of ruthenium (cf. the negative shift of the stripping peak and the variation in the peak shape). Performance loss due to Ru crossover is more pronounced for the cells operating at high relative humidity (Figure 4). This is in good agreement with the magnitude of ruthenium impact on the cathode, as indicated by CO stripping voltammetry in Figure 5.

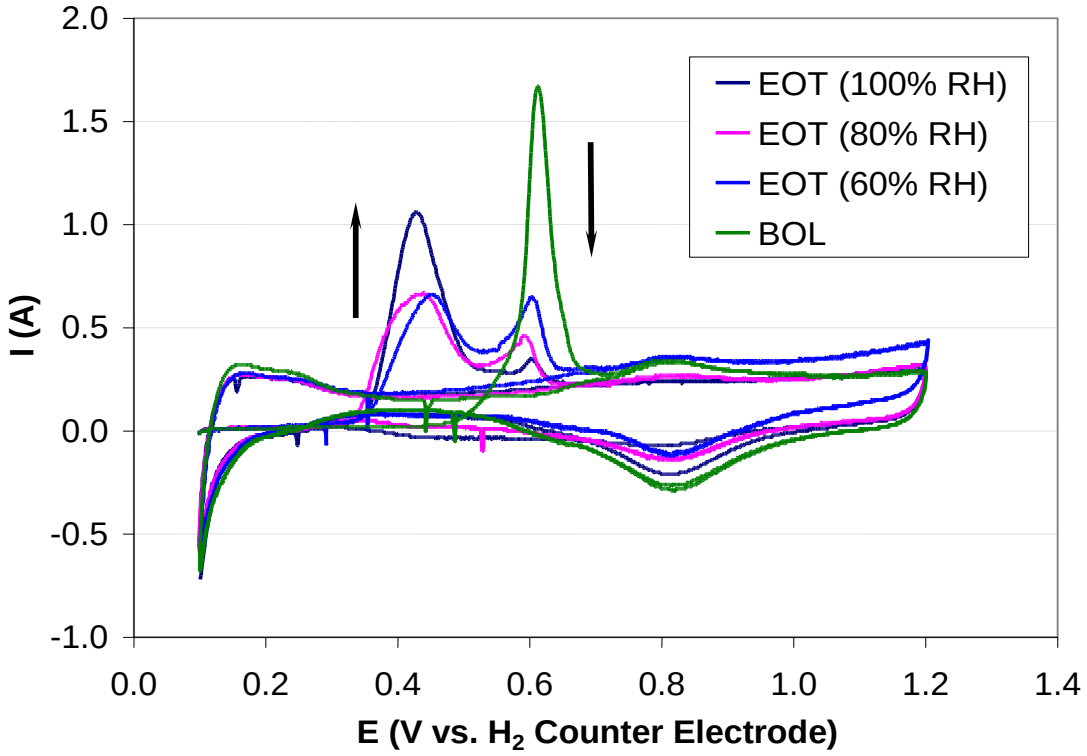

Figure 5. CO stripping voltammetry for the Pt cathode in a PEMFC operating on hydrogen reformate and PtRu anode after ASTs at different relative humidity [13].

In order to obtain more information about cathode catalyst changes, X-ray diffraction testing was performed. The results indicate no presence of a PtRu bulk alloy, which brings about the conclusion that Ru is deposited on the cathode surface. The amount of Ru accumulated during an AST of a PEFFC operating on hydrogen reformate at 100% relative humidity is very similar to the relative Ru quantities detected at DMFC cathodes [13]. Test results prove that ruthenium crossover is not restricted to DMFCs but also impacts other PEM fuel cells operating with a PtRu anode. Improvements in the anode stability and development methods of mitigation ruthenium deposition at DMFC cathodes may thus be also beneficial to reformate-fueled PEM fuel cells.

4 GOAL AND SCOPE

Ruthenium from binary PtRu catalysts undergoes dissolution from the anode due to thermodynamic instability in operating conditions. It migrates through the separating proton conducting membrane to deposit onto the cathode catalyst. As result of Ru deposition on the Pt catalyst, ORR activity of the cathode is greatly decreased. This negatively affects the fuel cell performance and creates a major obstacle for commercialization of fuel cells operating with PtRu anode catalysts.

The goals of this project are to evaluate the effects of ruthenium deposition on the cathode on the fuel cell performance, in particular:

- ruthenium migration from the anode with PtRu black catalyst,
- effect of ruthenium dissolution from the anode catalyst on methanol oxidation activity,
- changes in the Pt-to-Ru ratio at the anode,
- cathode contamination degree resulting from ruthenium contamination during manufacturing, humidification, and during fuel cell operation,
- changes in the cathode surface composition,
- cathode performance loss based on polarization curves,
- impact of Ru contamination on the oxygen reduction reaction (ORR) kinetics.

The project work has been carried out in single-cell fuel cells of active area of 5 cm^2 with a PtRu black anode catalyst, a Pt black cathode catalyst, and Nafion® 117 or Nafion® 1135 membranes.

The experimental part has consisted of:

- initial analysis of PtRu black and Pt black catalysts in order to verify the actual composition and loading with the X-ray fluorescence technique,
- MEAs and half-MEAs preparation using direct catalyst painting technique,
- fuel cell performance characterization at different operating times by polarization curves with hydrogen fuel and methanol fuel, anode polarization and methanol crossover experiments; these techniques allowed to compare initial performance with the state-of-the-art direct methanol fuel cell performance and determine cell degradation during the lifetime,
- evaluation of the active area of anode and cathode catalysts by using CO stripping technique, initially and at different points of interest, to probe ruthenium crossover and quantify the changes in anode and cathode catalyst activity in time,
- X-ray fluorescence of anode and cathode to record changes in catalyst composition from the initial state,
- oxygen reduction reaction in acidic media on Pt rotating disc electrode (RDE),
- spontaneous deposition of ruthenium on platinum RDE and oxygen reduction reaction in acidic media on ruthenium-contaminated platinum RDE to record changes in kinetics due to the presence of ruthenium.

The experimental part of this project will contribute to better understanding and quantification of the ruthenium crossover impact on ORR. In addition, the state-of-art performance degradation mitigation methods will be reviewed.

5 FUEL CELL PREPARATION

5.1 MEA preparation

The membranes used for DMFC MEA preparation were Nafion® 117 or two combined Nafion® 1135, which provided the same membrane thickness. The anode catalyst ink was prepared from HISPEC™6000 Pt: Ru black 50:50 atomic %, Nafion® 1105 from Du Pont, and Millipore 18.2 MΩ water. The calculated PtRu loading was 8 mg/cm^2. The cathode catalyst ink was prepared from HISPEC™1000 Pt black, Nafion® 1105 from DuPont and Millipore 18.2 MΩ water. The Pt calculated loading was 6 mg/cm^2. The active area was 5 cm^2. The catalyst layer was directly painted on the membrane. The two half-MEA's used for ruthenium crossover tests are shown in Figure 6.

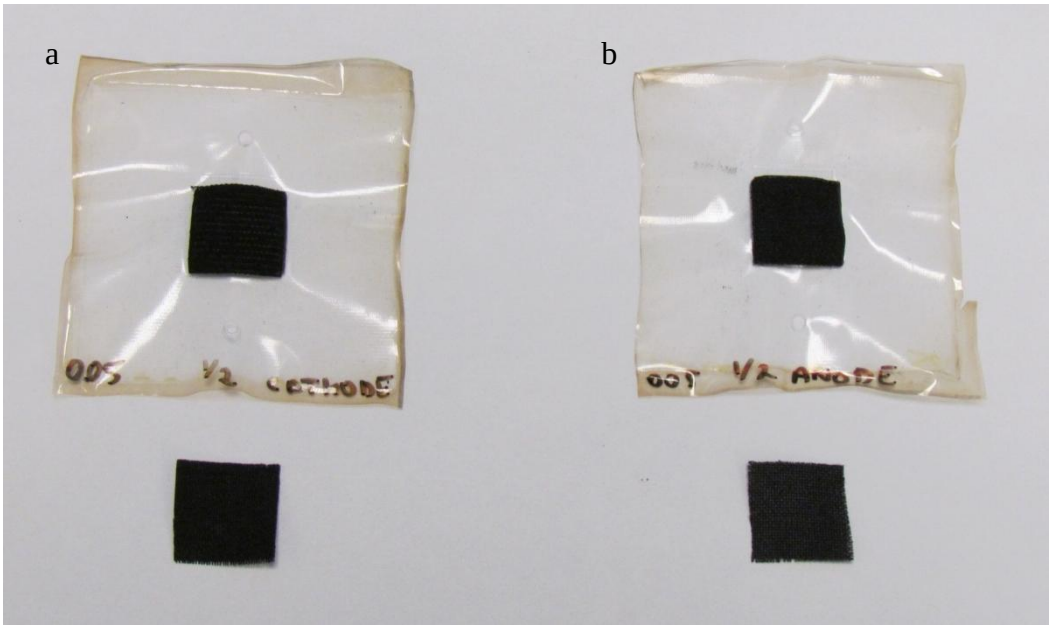

Figure 6. Half-MEAs for ruthenium crossover investigation a) half MEA with the cathode catalyst, Nafion® 1135 membrane and double sided carbon cloth GDL b) half MEA with the anode catalyst, Nafion® 1135 membrane and one sided carbon cloth GDL.

For ruthenium crossover evaluation a reference MEA was made with Pt black catalyst on both sides of the membrane at a loading as that used at the DMFC cathode (6 mg/cm^2). It was manufactured using direct catalyst painting on Nafion® 117 membrane, exactly the same way as MEAs with PtRu anode catalyst.

5.2 Fuel cell hardware

The MEA, the heart of the cell, was sandwiched between gas diffusion layers on both the anode and the cathode side. Gas diffusion layers were surrounded with gaskets, which provided sealing to prevent fuel and gas leakage and allowed system pressurization. Gas

diffusion layers and gaskets were different on the anode and cathode side. On the anode side, one-sided carbon cloth GDL (carbon/PTFE-blended Microporous Layer (MPL) applied to one side) was used together with a thinner gasket and on the cathode side, double-sided (carbon/PTFE-blended Microporous Layer (MPL) applied to both sides) carbon cloth was used together with a thicker gasket.

The MEA together with GDLs and gaskets was sandwiched between single-serpentine flow fields appropriate for a 5 cm^2 electrode surface area. The flow fields were attached to current collectors, which were further connected to an external circuit. The cell was compressed with eight screws using a torque of 100 pound-inch per screw. The fuel cell hardware together with a tested MEA and gaskets are shown in Figure 7.

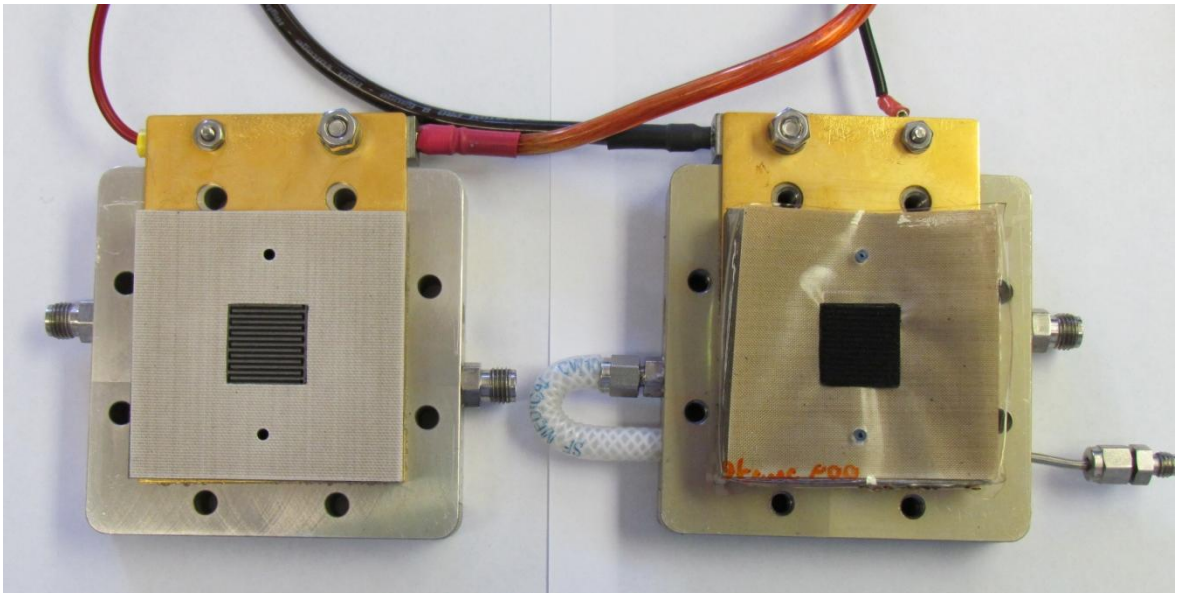

Figure 7. Cell hardware for fuel cell testing together with an MEA, gaskets, and gas diffusion layers.

6 TEST HARDWARE

6.1 Fuel cell test station

A fuel cell test station, manufactured by Fuel Cell Technologies (Albuquerque, New Mexico), capable of testing single cells or cell stacks generating a maximum voltage of 10 V and power of 150 W, was used for fuel cell testing in this work. The station was equipped with the load box, flow and pressure controllers, gas humidification bottles, and heaters. It was connected to a computer where data was collected. Parameter setting and test programs execution was done through a LabView software.

The test station together with a fuel cell being tested is shown in Figure 8. The anode and cathode gas flows were adjusted with automatic flow controllers or set manually using

rotometers. Their calibration was compensated for the ambient pressure of 0.76 bars due to Los Alamos altitude of 2300 m above sea level. There were two separate flow controllers, one for anode and one for cathode gas flow. Gases were directed to humidification unit where they are humidified at required temperature. After passing through a fuel cell, the gasses were directed through pressure controllers maintaining the required pressure level.

Cell temperature was controlled by a thermocouple and regulated by heaters inserted into endplates.

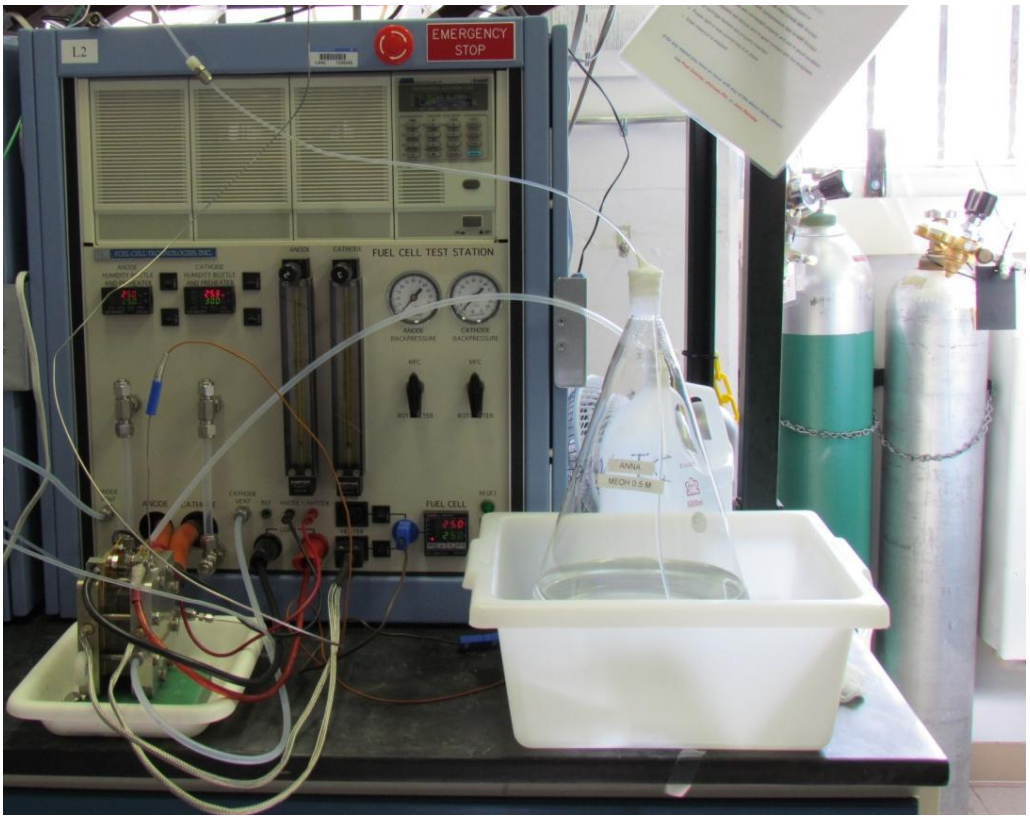

Figure 8. Single cell fuel cell test station with methanol supply and tested fuel cell.

6.2 Potentiostat

CO stripping experiments and CVs were executed using a Parstat 2273 potentiostat, equipped with a power booster. The rated current of the device was 10 A and voltage 20 V. The potentiostat was connected to the computer where data was collected. Experiments were carried out using Power Line software. The integration of current as a function of time to calculate the charge and, on that basis, determine the active area was done using an integrate software developed in house. The software was capable of integrating the area between two curves. Example integration results are shown in Figure 9.

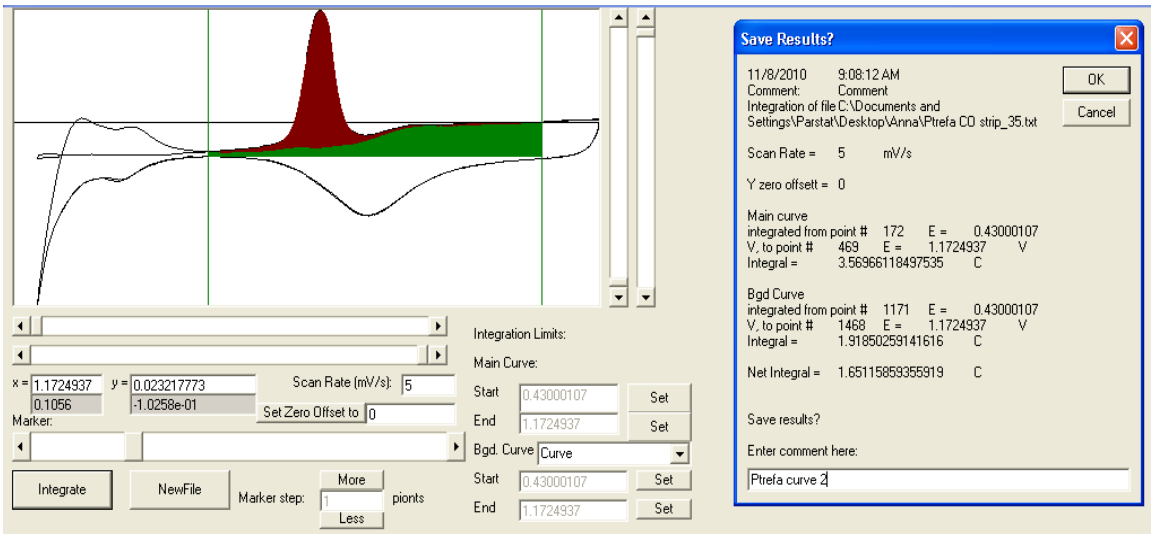

Figure 9. Example integration results obtained using "Integrate" software.

As shown in Figure 9, the program output was a total CO stripping charge. Integration limits and scan rate value could be manually adjusted.

6.3 Fuel supply

The methanol fuel concentration used in testing was 0.5 M. The concentration was checked using density/specific gravity/concentration meter DMA 4500. The measurements were executed at 20^{o}C. Methanol concentration was calculated from the equation given by the producer on the basis of measured density. Methanol fuel was supplied using solvent delivery module LC-10AD manufactured by Shimadzu with the maximum capacity of 1.8 mL/min.

6.4 Power source

Anode polarization and methanol crossover tests were carried out with the use of an external power source 6033A System Power Supply. The power source was capable of operating in either constant-voltage (0-20 V) or constant-current mode (0-30 A) at a maximum power of 200 W. It was used to generate voltage sweeps required in the anode polarization and methanol crossover experiments. Data was recorded on a computer using LabView 5.1.1 software.

7 FUEL CELL CHARACTERIZATION

Various characterization techniques were used to determine fuel cell performance as well as to distinguish and quantify performance losses such as related to fuel crossover,

activation, ohmic resistance and mass transport. In this work, the overall performance was characterized with j-V curves; fuel crossover was characterized using methanol crossover tests; anode activity was determined in anode polarization tests. For the purpose of determining fuel cell active area and ruthenium deposition on the cathode, CO stripping and cyclic voltammetry were used.

7.1 XRF catalyst characterization

Prior to fuel cell characterization, the anode and cathode catalyst loadings were experimentally verified with using of X-ray fluorescence (XRF). The measurements were performed on a Spectrace QuanX energy dispersive X-ray fluorescence analyzer equipped with a Cu filter and a liquid nitrogen cooled Si(Li) detector. The XRF results for the anode and cathode catalysts are summarized in Table 1.

Table 1. XRF measurements for anode and cathode catalyst loading and weight fraction in tested MEA for DMFC.

electrode	cathode	anode
loading [mg catalyst/cm2]	3.25	5.00
platinum [wt%]	99.96±0.996	63.11±0.638
ruthenium [wt%]	0.04±0.007	36.89±0.187

As shown in Table 1, the cathode catalyst loading was 3.25 mg Pt/cm^2 for the cathode catalyst and 5 mg PtRu/cm^2, which was approximately 60% of the expected (calculated) value. This indicates that catalyst ink losses during painting process were larger than assumed in calculations. Interestingly, the cathode catalyst shows detectable amount of ruthenium already after MEA preparation. The anode Pt-to-Ru ratio was found to be approximately 63:37 wt%.

7.2 Polarization curves

The j-V polarization curves were the primary in-situ characterization technique. The current density and voltage provide information about activation, ohmic, and mass transport losses. The j-V curves can be determined in either a constant-voltage or constant-current modes. For the purpose of this work, a constant-voltage mode was used. The voltage was changed from an open circuit to 0.2 V with a step of 0.1 V and delay time of 120 seconds for each point. Polarization curves were determined using both hydrogen and methanol fuel. Before taking the j-V curve, fuel cells were “broken-in” for 120 min at constant voltage of 0.7 V. The cathode gas was air. The test conditions for hydrogen and methanol are shown in Tables 2 and 3 respectively.

Table 2. Testing conditions for hydrogen fuel j-V characterization.

Fuel	Hydrogen
Fuel flow rate [sccm]	200
Oxidizer	Air
Oxidizer flow rate [sccm]	500
Anode humidification temperature [^{o}C]	105
Cathode humidification temperature [^{o}C]	90
Cell temperature [^{o}C]	80
Anode backpressure [psig]	20
Cathode backpressure [psig]	20
Compression torque [pound inch]	100

Table 3. Testing conditions for methanol fuel j-V characterization.

Fuel	methanol
Fuel concentration [Molar]	0.5
Fuel flow rate [ml/min]	1.8
Oxidizer	Air
Oxidizer flow rate [sccm]	500
Anode humidification temperature [^{o}C]	n/a
Cathode humidification temperature [^{o}C]	90
Cell temperature [^{o}C]	80
Anode backpressure [psig]	n/a
Cathode backpressure [psig]	0
Compression torque [pound inch]	100

The polarization curves (not iR-corrected) recorded after the "break-in" of the cell are shown in Figures 10 and 11 for hydrogen and methanol fuel, respectively.

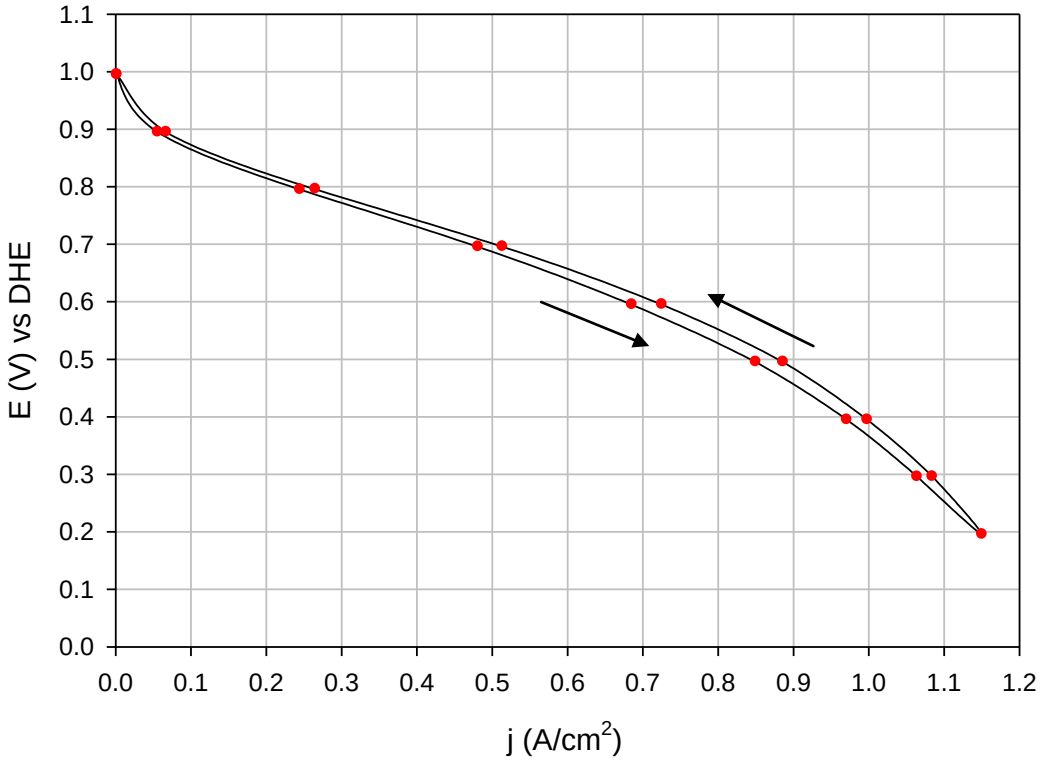

Figure 10. j-V curve for hydrogen fuel characterization.

Characteristic performance metrics recorded for the hydrogen fuel operation mode were as follows: open circuit voltage of ~ 1.0 V vs. DHE, current density of 0.5 A/cm^2 at 0.7 V, and high frequency resistance (HFR) of 0.176 Ω cm^2. The delay time between each point ensured a steady state during measurements, however some hysteresis can be seen. The current densities observed in the reverse potential sweep are higher than in the first sweep from open circuit down to 0.2 V. This is due to the platinum oxidation state. In OCV conditions, when cathode potential is high, platinum is oxidized. Moving to the high current region causes a cathode potential drop and the reduction of surface oxides. The reduced platinum surface shows increased activity in the reversed sweep.

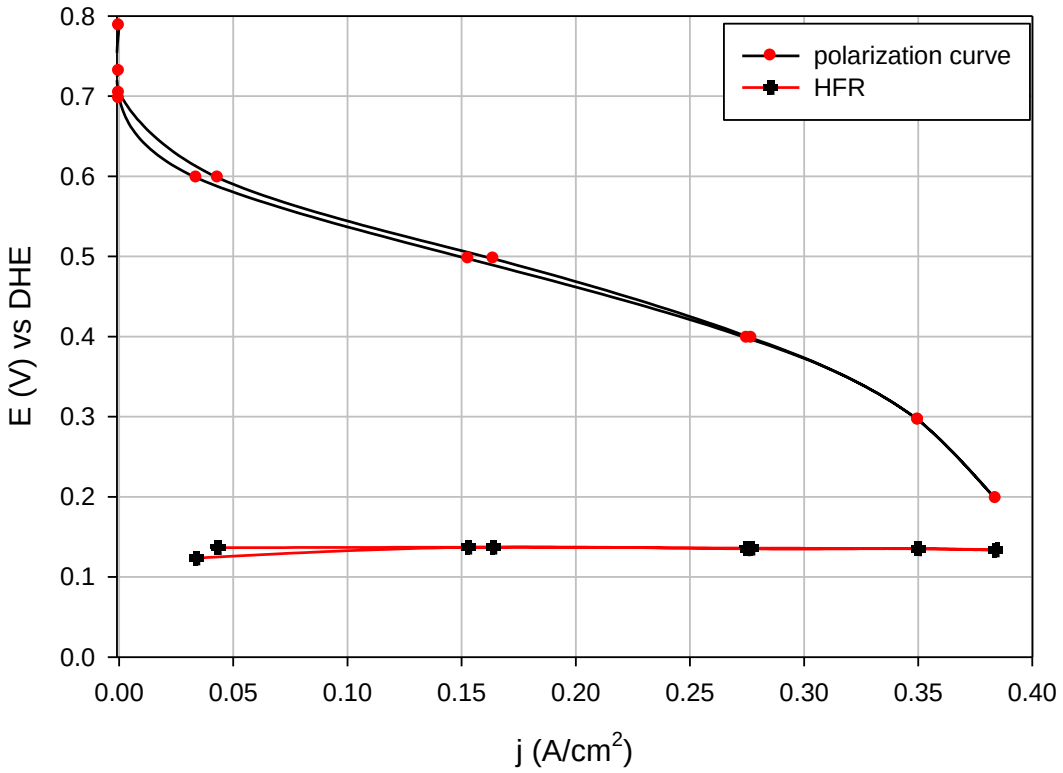

Figure 11. j-V curve for methanol fuel cell characterization at cell temperature of 80°C and 0.5 M methanol.

Characteristic performance metrics recorded for methanol fuel operation mode were as follows: open circuit potential of 0.8 V, current density of 0.16 A/cm^2 at 0.5 V, HFR of 0.144 Ω cm^2.

The DMFC performance metrics are lower than when hydrogen fuel is used. Open circuit voltage was found to be approximately 0.2 V lower than in the H_2-air fuel cell due to methanol crossover. The maximum current density is roughly two times smaller due to sluggish kinetics of both methanol oxidation at the anode and oxygen reduction at the cathode, which additionally suffers from methanol crossover.

The polarization curve hysteresis in Figure 11 was marginal, which proves that 120 sec delay between data points is sufficient to stabilize methanol crossover at an altered potential and provide steady state conditions for j-V curve measurements.

7.3 Anodic polarization

The anodic polarization is an in-situ characterization technique which provides data about the anode ability to oxidize the fuel and allows for the determination of the limiting current density of the anode process. In this work, the anode activity was determined for methanol fuel. In anode polarization experiments the fuel cell cathode was supplied with hydrogen to serve as a reference electrode. Test conditions are shown in Table 4.

Table 4. Anodic polarization test conditions.

Anode supply	0.5 M methanol
Anode flow rate [ml/min]	1.8
Cathode supply	Hydrogen
Cathode flow rate [sccm]	200
Anode humidification temperature [^{o}C]	n/a
Cathode humidification temperature [^{o}C]	90
Cell temperature [^{o}C]	80
Anode backpressure [psig]	n/a
Cathode backpressure [psig]	20
Compression torque [pound inch]	100

During the experiment, current density was measured in the potential range of 0.15 V to 1.0 V vs. dynamic hydrogen reference electrode (DHE) with a potential step of 0.01 V. Anodic polarization test results (iR-corrected and not iR-corrected) are shown in Figure 12.

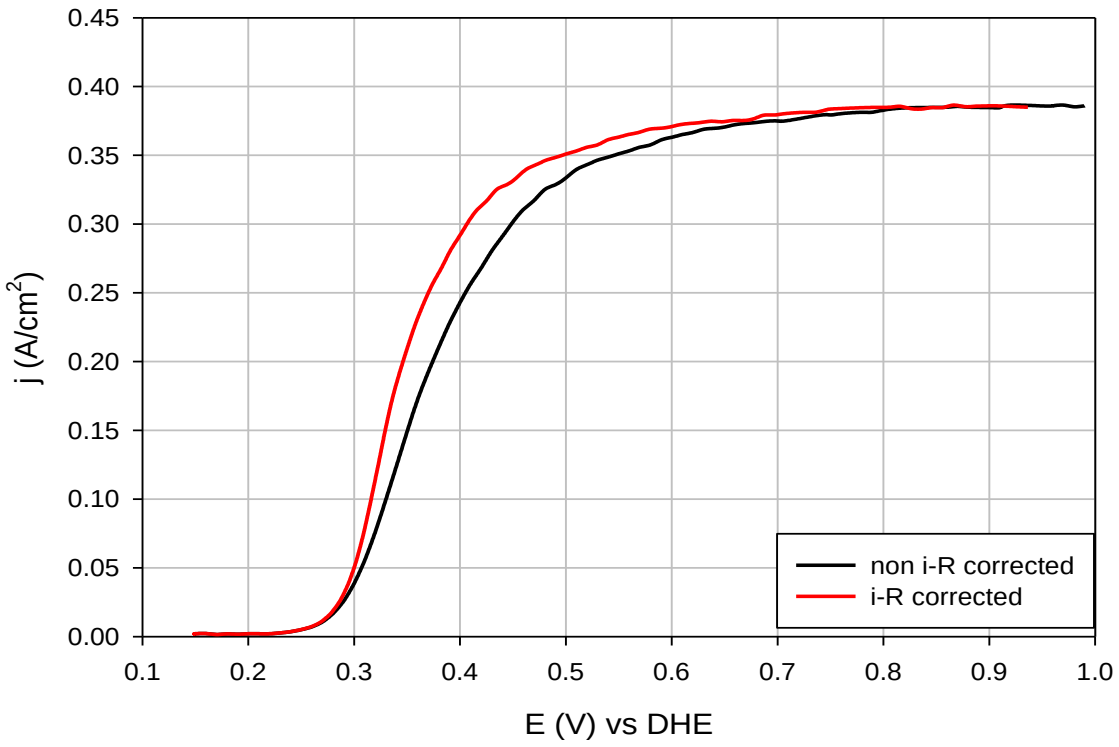

Figure 12. Anodic polarization test results.

As shown in Figure 12, the limiting current of methanol oxidation is approximately 0.38 A/cm^2. The half-wave potential for iR-corrected results is 0.34 V vs. DHE.

7.4 Methanol crossover test

Methanol crossover test provided information about the fuel permeation from the anode to the cathode side. It was performed with the use of a test station. The cell anode was supplied with 0.5 M methanol, the cathode side was supplied with ultra high purity (UHP) nitrogen. Cell voltage was swept using an external power source from 1.0 V down to 0.2 V with a step of 0.01 V. The current density reflecting the amount of methanol being oxidized on the cathode was recorded. Conditions maintained during methanol crossover determination are shown in Table 5.

Table 5. Test conditions for methanol crossover.

Anode supply	0.5 M methanol
Anode flow rate [ml/min]	1.8
Cathode supply	Nitrogen
Cathode flow rate [sccm]	200
Anode humidification temperature [^{o}C]	n/a
Cathode humidification temperature [^{o}C]	90
Cell temperature [^{o}C]	80
Anode backpressure [psig]	n/a
Cathode backpressure [psig]	0
Compression torque [pound inch]	100

The plot of crossover current density versus cell potential is presented in Figure 13.

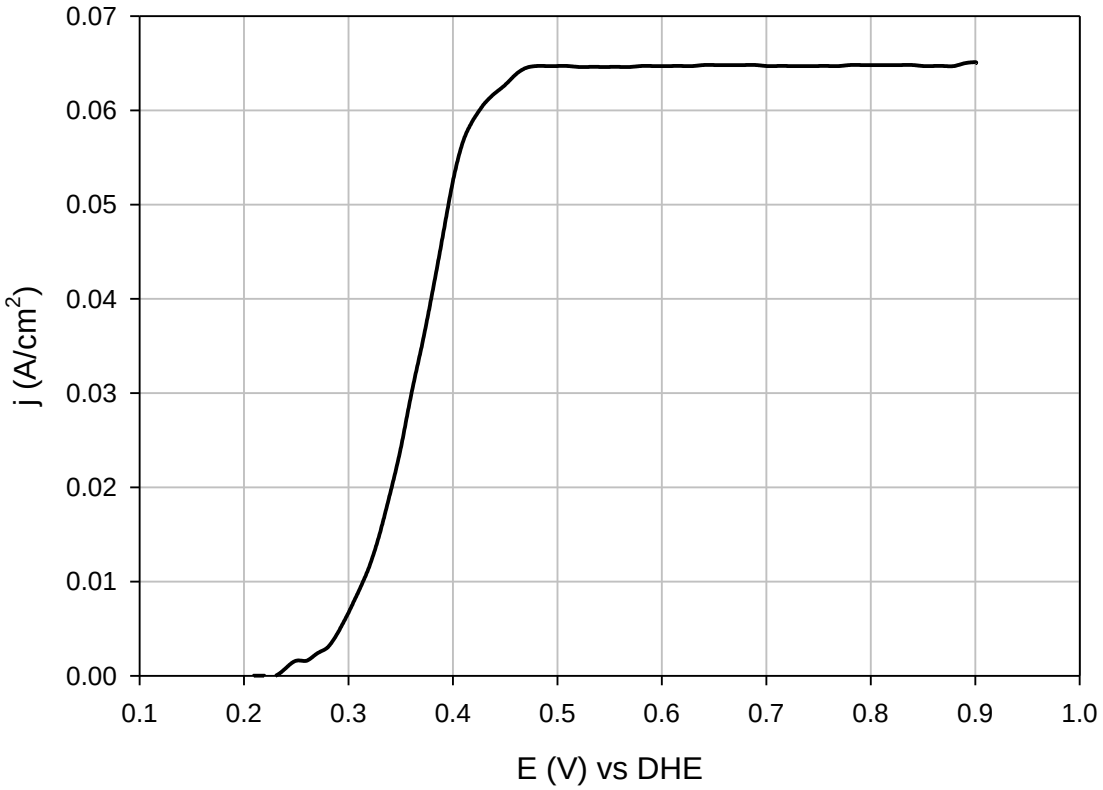

Figure 13. Methanol crossover test results.

As shown in Figure 13, for anode operating conditions corresponding to the OCV of the fuel cell, methanol crossover current density is the highest which is in good accordance with information presented in Chapter 2. The recorded crossover current density value for 0.5 M methanol concentration is 65 mA/cm^2, which is in good agreement with results obtained in [14].

Knowing the crossover current density, the amount of methanol fuel being oxidized on the cathode can be calculated using Equation 4.

$$N_{methanol} = \frac{j_{crossover} A_{active}}{nF}, \qquad (4)$$

where:

$N_{methanol}$-number of mols of methanol oxidized on the cathode [mol/s]

$J_{crossover}$-current density [A/cm^2]

A_{active}-active area [cm^2]

n- number of electrons released per one molecule of fuel

F- Faraday constant.

For a crossover current density of 65 mA, the methanol fuel crossover was calculated to be $5.6 \cdot 10^{-7}$ mol/s which can be further converted to 0.08 ml/h which is 0.07% of total supplied fuel.

8 RUTHENIUM CROSSOVER IN DMFC

8.1 CO stripping voltammetry technique

CO stripping voltammetry is an electrochemical experimental technique which provides information about the real active area of the catalyst. “Real surface area” in reference to fuel cell electrodes means the surface area of metal particles which are in contact with electrolyte and the current collector simultaneously [15]. The term can refer to either the anode or cathode catalyst of a fuel cell. The information about active area size is very important in durability studies where by comparing active area at different times of the cell lifetime it is possible to correlate active surface area loss to performance degradation. For pure platinum catalysts the active surface area can be determined from the hydrogen desorption charge, however CO stripping voltammetry is more widely applicable and it is also suitable for the determination of the surface area of PtRu catalysts.

8.1.1 CO stripping method uncertainties

When interpreting CO stripping experiment results, it is important to be aware of uncertainties of this method and to estimate the errors that occur due to various effects.

In order to determine the electrochemically active area, the CO stripping curve achieved experimentally needs to be integrated. During the integration process double layer charging current needs to be subtracted from CO oxidation results. The value of double layer current is obtained from cyclic voltammetry in nitrogen. CVs of PtRu catalysts are difficult to integrate accurately due to the fact that the oxide formation region overlaps with the CO stripping peak. The second effect which can contribute to the integration errors is the charge in the oxide-formation region which can involve also charges of the oxidation of impurities adsorbed in the process of CO adsorption and the in oxide-formation charge itself. Those effects give a raise to different current values at high potentials in the first and the second potential sweeps.

Another uncertainty of the CO stripping method is related to the type of a bond that CO forms on the surface, which affects active area calculation. In this work, the active area is calculated from Equation 5.

$$S_{CO} = \frac{Q_{CO}}{0.420\ mC/cm^2} \quad (5)$$

where Q_{CO} is the CO stripping charge determined by integration of CO stripping curve and $0.420\ mC/cm^2$ is a charge corresponding to a monolayer of chemisrobed CO.

The value used in Equation 5 is correct if all CO adsorbed forms a linear bond. According to [16], for polycrystalline platinum, CO is mostly linearly bonded, which means that the use of $0.420\ mC/cm^2$ for the CO monolayer charge should not lead to significant errors.

Because of the integration uncertainties associated with the CO charge determination on platinum surface, the real surface area of cathode catalyst determined from the CO stripping experiments was often compared with results obtained from hydrogen adsorption charge integration. This helped to estimate the experimental error of the surface-area measurements and to ensure that experimental error does not severely affect the research outcomes or lead to incorrect conclusions.

CO stripping experiment results are also dependent on CO adsorption time, sweep rate and adsorption potential. In this work, only the effect of adsorption time was studied. According to [15] a saturated CO monolayer is achieved after 15 minutes of adsorption and extension of that time to 30 minutes results in marginal differences in CO stripping experiment outcomes which can be assigned to experimental error. This information was verified by performing CO stripping for different adsorption times. It was found out that 10 min adsorption time results in marginal differences in CO coverage compared with 20 min adsorption time and 30 min adsorption time (5 min adsorption appeared too short). The effect of the CO stripping adsorption time on CO coverage is shown in Appendix A.

According to [16], the CO adsorption potential which yields a monolayer CO coverage is 0.1 V vs. RHE. It was also found in [15] that the use of high CV sweep rates can cause a shift in the CO stripping peak potential and result in underestimated CO stripping charges. The maximum charge and minimum peak potential were obtained with a sweep rate of 5 mV/s. That sweep rate was used in experiments without an additional verification.

8.2 Currentless ruthenium crossover

8.2.1 Experimental

The cell described in Chapter 5 was connected to a test station and supplied with humidified hydrogen and air at flow rates of 200 sccm and 500 sccm, respectively, and backpressures of 20 psig for both the anode and the cathode side. The cell temperature was 80^{o}C; humidification bottle temperatures were 105^{o}C for the anode and 90^{o}C for the cathode. The cell was maintained at OCV for two hours. Next, the cell was cooled down to 25^{o}C and CO stripping votammetry performed. The cell was connected to a Parstat 2273 potentiostat and a computer. Data was recorded using Electrochemica software.

Before, the CO adsorption process, the cathode was purged with the humidified nitrogen until potential dropped to the level of 0.1-0.15 V. The nitrogen purging procedure was performed in order to remove air. The anode was supplied with humidified hydrogen throughout the cathode CO stripping voltammetry experiment and served as a DHE reference electrode. After the purging procedure was completed, the CO adsorption process was started. The cathode feed was switched from nitrogen to a 1% CO mixture with nitrogen of ultra high purity. The potential was held at 0.1 V vs. DHE for 120 seconds in order to initially adsorb CO. Then, the potential was switched to 0.9 V for 60 seconds and CO together with impurities which might have been adsorbed on platinum surface was oxidized. The purpose of this procedure was to clean the surface and ensure that all available platinum sites were available to CO. After cleaning procedure was completed, the potential was switched back to 0.1 V vs. DHE for 20 minutes in order to adsorb CO on the surface. After the CO adsorption process was completed, the cathode flow was switched back to nitrogen for 20 minutes to purge non-adsorbed CO and have only a monolayer of adsorbed CO left.

The CO adsorption process was followed by CO stripping voltammetry. The potential was swept from 0.1 V to 1.3 V and back at a scan rate of 5 mV/sec. After the CO stripping, an additional CV was performed to ensure complete CO removal and provide a baseline for charge integration and method error estimates. The CO stripping procedure and conditions were the same in all experiments.

After the first CO stripping experiment, the cell anode was supplied with 0.5 M methanol at the flow rate of 1.8 mL/min and cell cathode was supplied with air at the flow rate of 500 sccm at humidification temperature of 90^{o}C and backpressure of 20 psig for two hours. The cell temperature was kept at 80^{o}C. Next, the cell was cooled down to 25^{o}C and CO stripping voltammetry procedure was performed. The procedure consisting of two hours period cell supply with methanol-air at OCV conditions and performing CO stripping voltammetry afterwards was repeated until consistency in achieved results was reached.

The results of the cathode current-less ruthenium contamination were compared with CO stripping voltammetry results obtained for a Pt-Pt reference MEA cell of equal active area and platinum loading consistent with investigated cathode.

8.2.2 Results and discussion

The results of the CO stripping experiment for the current-less ruthenium crossover evaluation are shown in Figure 14, where (a) shows CO stripping voltammetry results and (b) respective cyclic voltammetry results in the absence of CO.

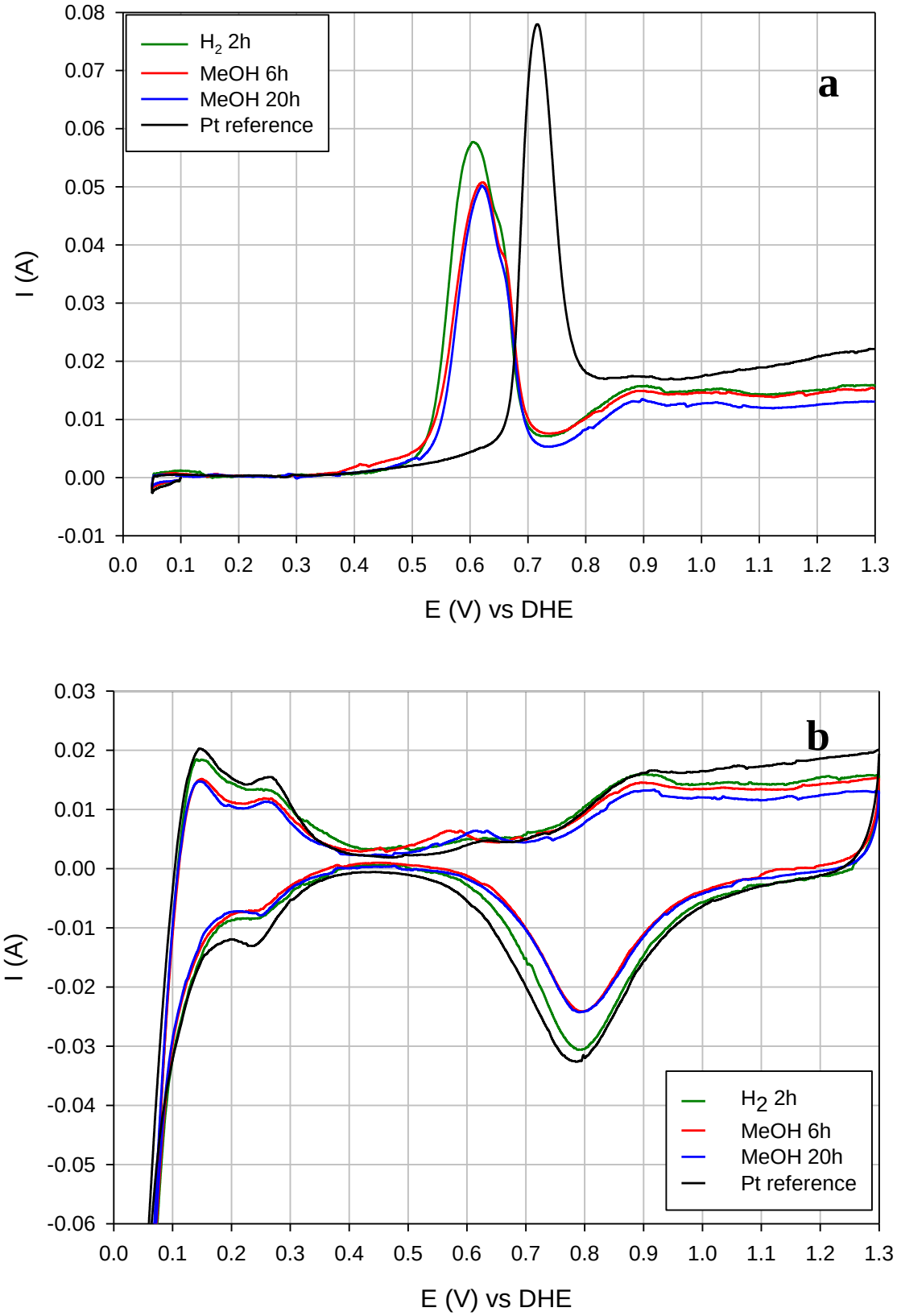

Figure 14. Cyclic voltammetry from currentless Ru crossover testing: (a) CO stripping scans and (b) cathode CVs in the absence of CO.

The experiments reveal the presence of Ru at the cathode after only two hours of H_2-air fuel cell operation. Further operation on methanol does not increase the cathode contamination. The CO stripping peaks recorded after current-less operation on methanol-air are shifted positively by 20 mV with respect to the CO stripping peak obtained after current-less hydrogen-air operation. The overall (after initial operation on hydrogen and methanol) negative shift in CO stripping peak potential, resulting from current-less contamination was determined to be 100 mV.

In order to analyze CO stripping results in more detail, the plot of CO stripping peak potential versus contamination time is presented in Figure 15.

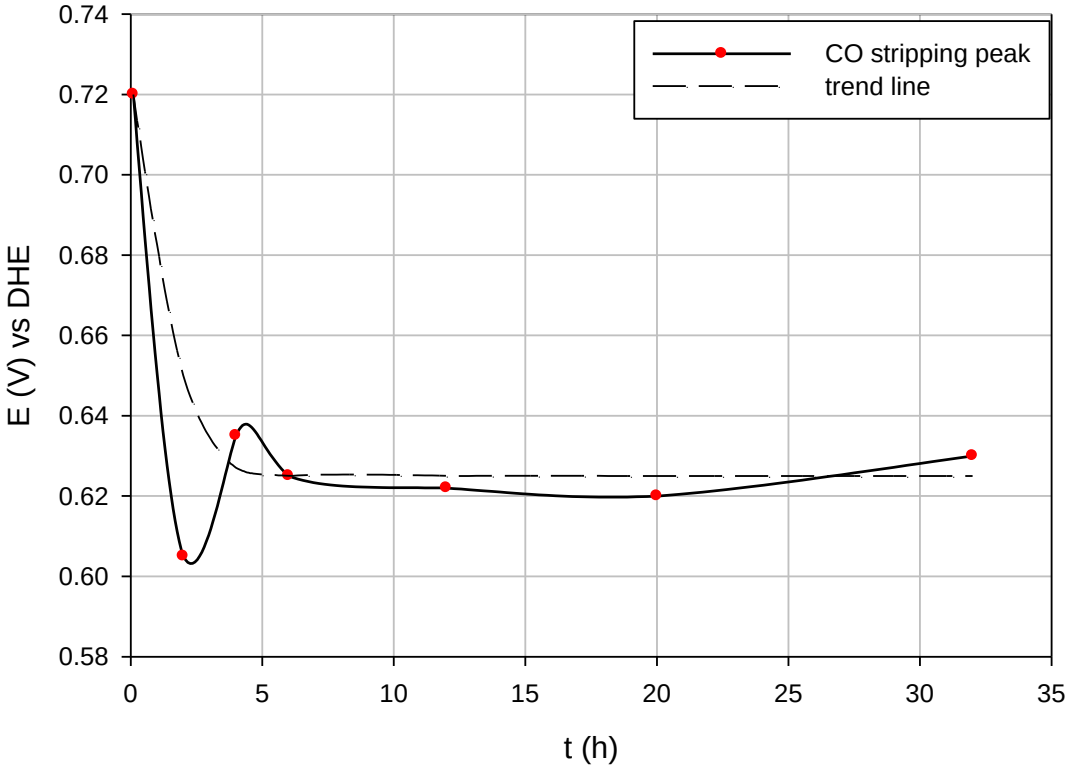

Figure 15. CO stripping peak potential plot versus time.

The current-less ruthenium contamination trend line indicates an exponential decay with time. It is hard to precisely determine how fast the contamination had happened because it was completed before the first data point was taken. The positive shift of CO stripping peak potential after the fuel change from hydrogen to methanol is not fully understood. Some possible explanations were found in literature. It was reported in [11] that potential cycling within 0.1 V to 1.3 V vs. SHE can result in a positive CO stripping potential shift. After 10 cycles at 5 mV/sec scan rate, a 35 mV shift was recorded. Moreover, a 20 mV positive shift of CO stripping peak was observed for six-cell stack after 100 h of DMFC operation mode. This effect was assigned to ruthenium removal due to prolonged high

potential of air cathode. However, in this research, the positive shift was observed after only two hours of DMFC operation mode.

A possible explanation could be that methanol crossover causes a decrease of cathode potential thus contributing to reduction of platinum and average ruthenium oxidation state (ruthenium hydroxides). Since Pt and Ru hydroxides benefit CO stripping rate, this effect would tend to shift the CO stripping peak in a positive direction.

The results for current-less ruthenium crossover obtained in [11] confirm that the contamination occurs quickly after humidification. The exact time of humidification before CO stripping experiment was not reported. Contrary to this study, the cell cathode in [11] underwent CO stripping without being exposed to hydrogen or methanol first. The current-less ruthenium contamination level in [11] seems to be higher as the CO stripping peak potential occurs at approximately 0.5 V compared to 0.625 V obtained in this study. The results however are not fully comparable due to differences in procedures applied.

When analyzing the current-less ruthenium contamination, it is important to take into account that it includes the contamination during MEA preparation which in turn depends on chosen preparation technology. According to [11], the smallest current-less ruthenium contamination is achieved when MEA is prepared using a decal transfer method on two 1135 Nafion® membranes stacked together in a fuel cell. This method, however, is lengthy and it was substituted with the direct painting of catalyst on Nafion® 1135 membranes, which still led to better results compared to using a single Nafion® 117 membrane.

In order to verify the CO stripping results, a comparison of specific active surface area [m^2/gPt] obtained from hydrogen charge integration and carbon monoxide charge integration was made. Ruthenium was treated as if it formed the same type of a surface bond as on Pt. The plot of specific active surface area versus time is shown in Figure 16.

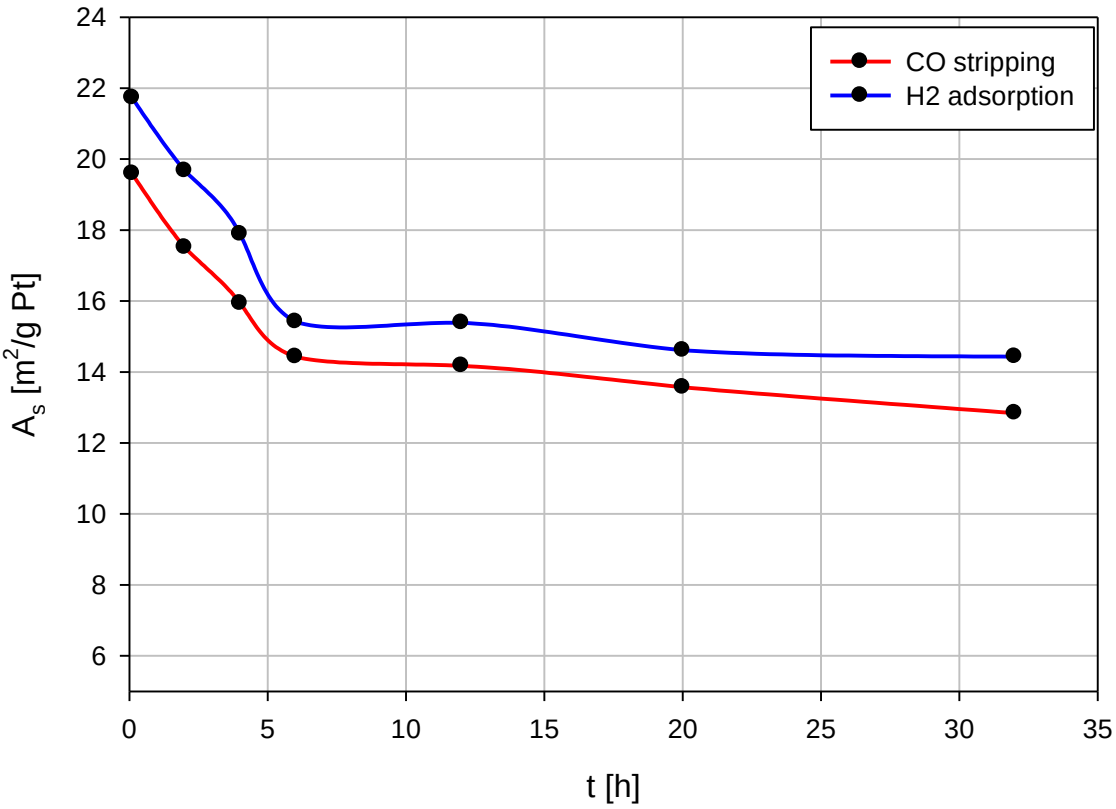

Figure 16. Comparison of specific active area obtained from integration of hydrogen charge and carbon monoxide charge.

As shown in Figure 16, CO stripping charge decreases in time. The rate of the decay changes in time and may be approximated with two linear regions: fast initial degradation within the first 6 hours, followed by much slower decrease later on. The active area reduction might be caused by catalyst particles agglomeration and sintering.

The results were obtained from integration of hydrogen charge and carbon monoxide charge with the use of the integration software. The total charges measured were divided by specific charge: 2.1 C/m^2 for hydrogen and 4.2 C/m^2 for carbon monoxide adsorbed on platinum surface. The calculated surface area was divided by total platinum loading of 15 mg in order to achieve specific active surface area. It is shown that the values obtained in hydrogen and CO experiments are in good agreement. The average relative difference is ~9%.

The specific active area obtained from CO stripping charge integration is consistently lower than the active area obtained from hydrogen desorption charge integration. One possible explanation is that there are highly oxidized ruthenium species present on the cathode surface. According to [19] those species do not adsorb CO thus are not detected by CO stripping. They block Pt sites from adsorbing CO, which results in lower surface area detectable by CO stripping. Another possible explanations are that the CO coverage was not complete or that the error occurred during integration process.

Overall, the two methods gave similar enough results for the surface area determination to be considered accurate and valid.

8.3 Current-assisted ruthenium crossover testing

8.3.1 Experimental

The most significant cathode contamination with ruthenium takes place under operating conditions with current flow. In order to investigate the effect of current-assisted contamination, an anode-potential-hold experiment was performed. The experiment was continued on the same cell, starting from the point when current-less contamination reached a saturation level. The anode was supplied with 0.5 M methanol at the flow rate of 1.8 mL/min and cathode was supplied with hydrogen at flow rate of 200 sccm, at 20 psig backpressure. The cell temperature during the experiment was 80^{o}C.

The anode potential was held at 0.2 V vs. DHE for two hours and the current was measured. Afterwards, the CO stripping experiment for the cathode was performed in order to assess the cathode contamination change. The same procedure was repeated for anode potential holds at 0.3 V, 0.4 V, 0.5 V, 0.7 V, 0.9 V, 1.1 V, and 1.3 V. Following the anode potential hold at 1.3 V and the ensuing CO stripping from the cathode, the CO stripping experiment for the anode was also performed. Next, the potential was held at 1.3 V and CO stripping experiments for the cathode and anode followed until the CO stripping peak potential and charge reached equilibrium.

8.3.2 Results and discussion

The CO stripping voltammetry results and respective CVs in the absence of CO are shown in Figure 17.

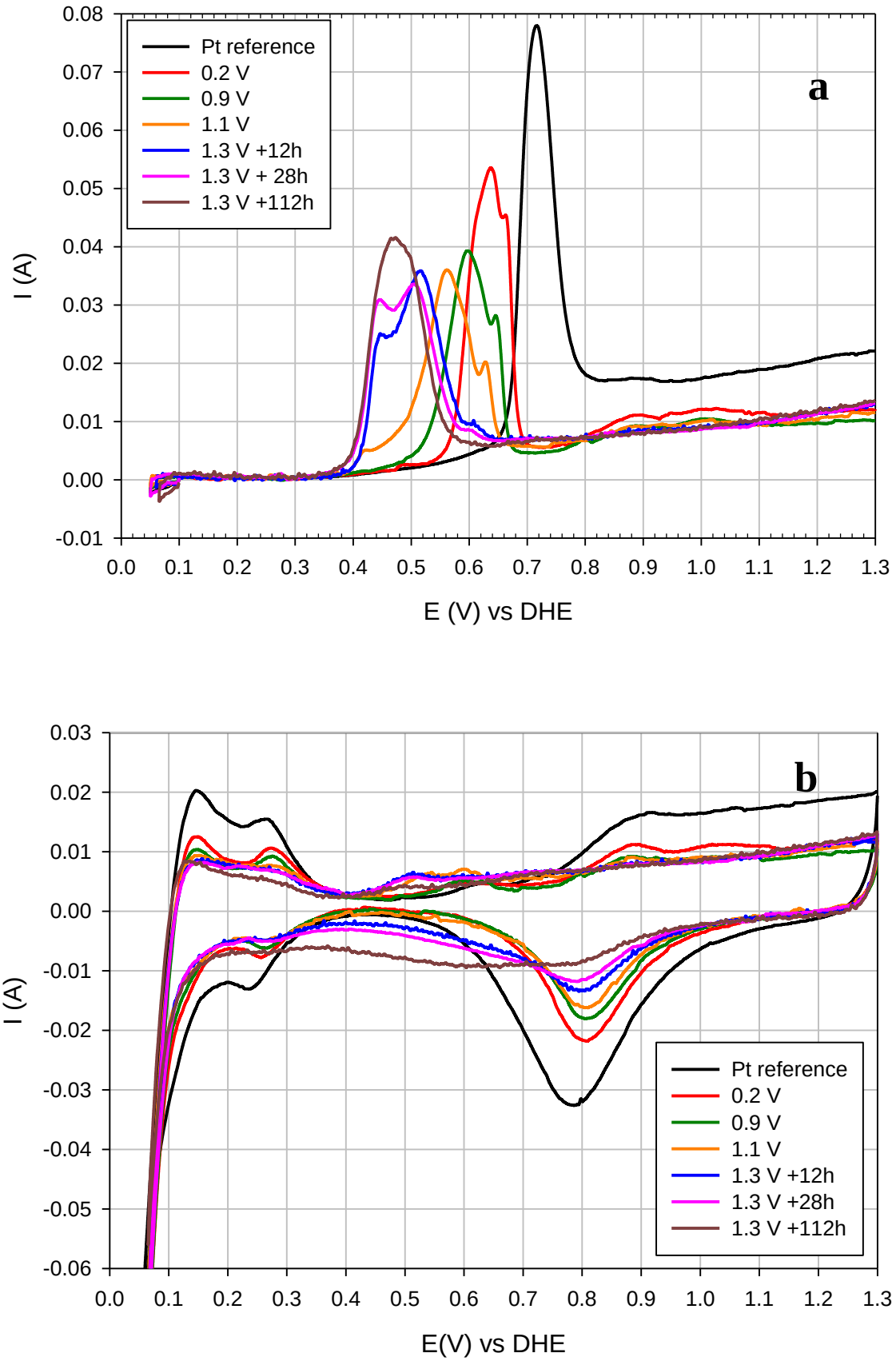

Figure 17. Cyclic voltammetry from current-assisted Ru crossover testing: (a) CO stripping scans and (b) cathode CVs in the absence of CO.

CO stripping peaks in Figure 17a shows a negative potential shift after the anode potential hold at 0.9 V vs DHE. The negative shift increases after the anode potential hold at 1.1 V and at 1.3 V. The negative shift continues with the prolonged anode potential hold at 1.3 V, however, the shift rate is much decreased. The CO stripping peak potential reaches a steady state at 0.49 V vs. DHE after 112 hours of holding the anode potential at 1.3 V.

The negative shift of the cathode CO stripping peak potential results from the ruthenium presence. The ruthenium content in cathode catalyst increases with time for anode potential holds at 0.9 V and at higher potentials until the cathode state reaches a steady state and ruthenium content does not increase anymore. CO stripping from a highly Ru-contaminated cathode starts resembling a CO stripping form a PtRu anode. Cyclic voltammograms indicate that surface-oxide reduction reaction is severely limited by the presence of ruthenium. The oxide reduction peak, initially present at a potential of ~ 0.8 V, flattens out with increasing Ru presence. It indicates that due to deposited ruthenium, some of the platinum sites are no longer available and the oxide reduction reaction can no longer take place.

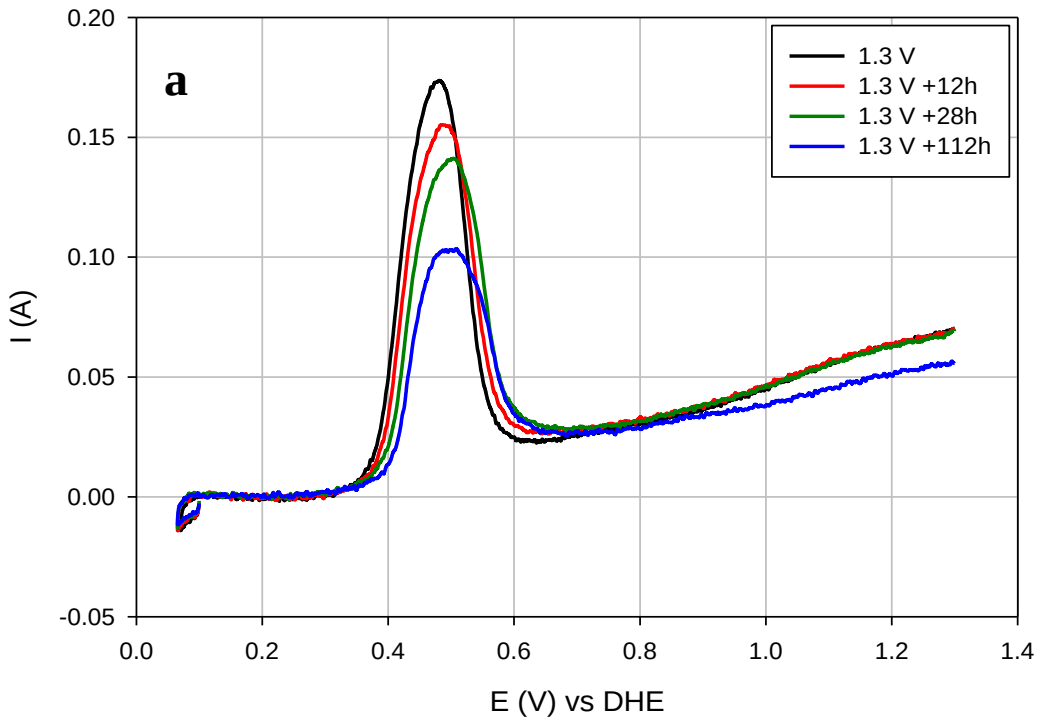

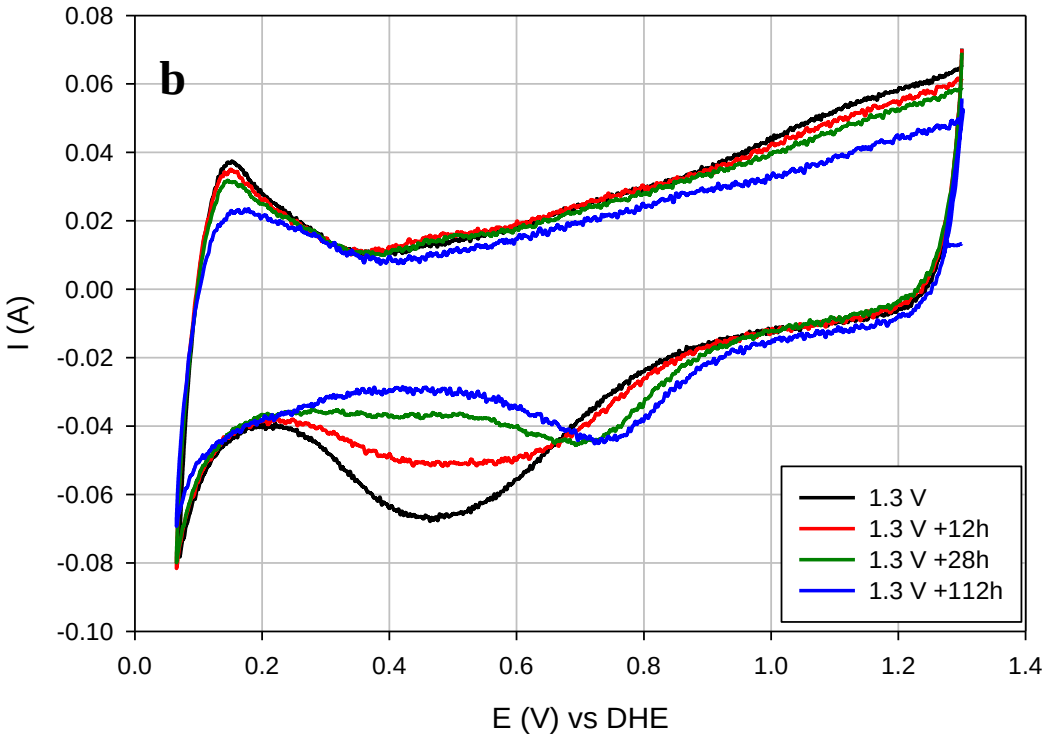

Figure 18. PtRu anode voltammetry at different stages of the current-assisted Ru crossover test: (a) CO stripping scans and (b) CO-free CVs.

The reduction in electrochemically-active platinum sites is also reflected by a decrease in the hydrogen adsorption charge and significant increase in the double-layer charging current. Ruthenium crossover has also an effect on the anode catalyst. The results of CO stripping from the PtRu anode catalyst (Figure 18a) and cyclic voltammograms of the CO-free anode are shown in Figure 18b.

According to Figure 18a, the anode CO stripping peak potential does not show any significant positive potential shift, however the CO stripping charge decreases with time which represents catalyst activity reduction and might be a result of catalyst particles agglomeration and/or ruthenium loss. The cyclic voltammogram scans indicate the shift in oxide reduction peak to more positive potential. It could be resulting from more platinum sites exposed on the catalyst surface due to the loss of ruthenium from anode catalyst, however it should be accompanied with positive CO stripping peak potential shift which was not observed.

Cathode and anode CO stripping potential shifts in time are shown in Figure 19.

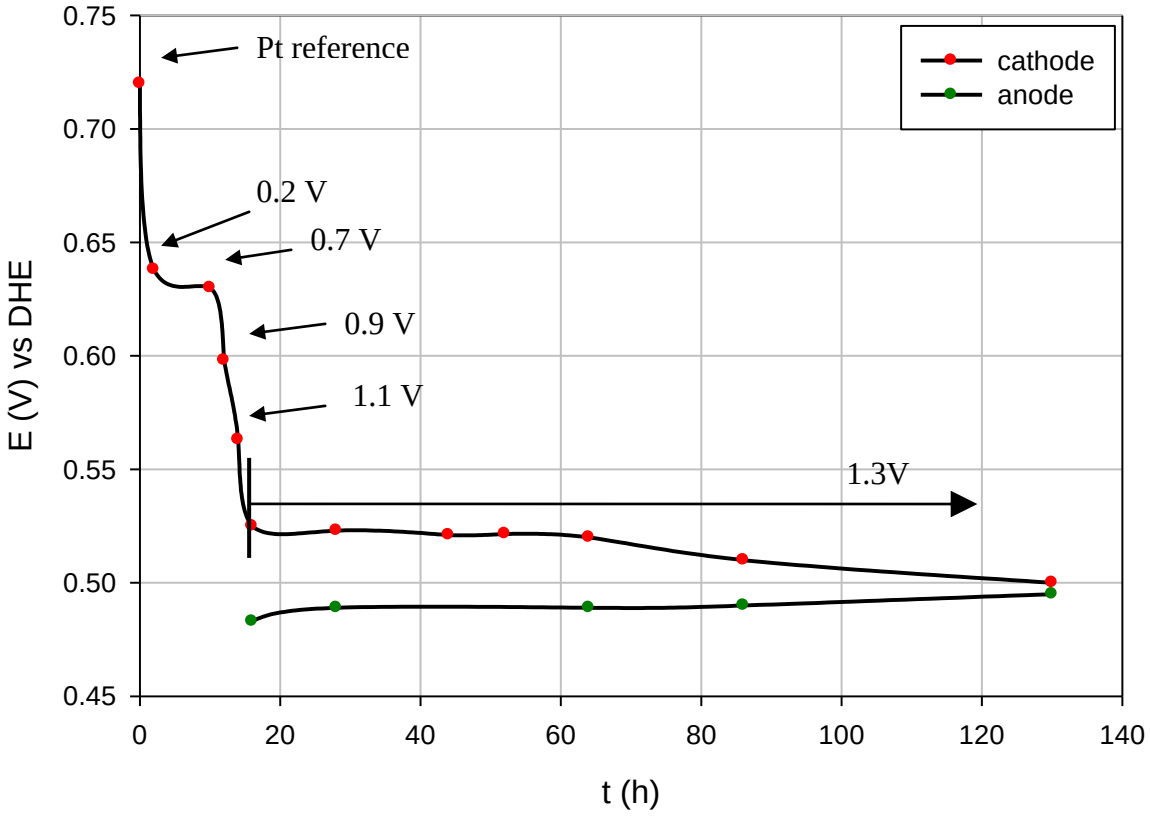

Figure 19. Cathode and anode CO stripping potential change in time during anode polarization experiment.

The total positive shift in anode CO stripping peak is limited to 12 mV. The shift may result from a loss of ruthenium from the catalyst surface or from the catalyst particle growth caused by potential cycling.

An initial drop of the cathode CO stripping potential of 101 mV within first two hours represents the current-less ruthenium contamination. In the next 10 hours, the CO stripping peak potential remains almost unchanged and this period reflects increasing anode potential up to 0.9 V vs. DHE. After the anode potential had reached 0.9 V and was being further increased up to 1.3 V, the cathode CO stripping potential had already dropped by 130 mV. With prolonged anode potential hold at 1.3 V the cathode CO stripping peak shows mostly change in shape, resulting from the change in catalyst surface morphology as shown in Figure 18a. It finally reaches a single-peak shape and remains within only 10 mV of the anode CO stripping peak.

Accurate determination of the CO stripping peak potential for the cathode was challenging. The peak was clearly split into two smaller peaks, one caused by CO oxidation on platinum near ruthenium and ruthenium itself, and one by CO oxidation on platinum-rich part of the surface. Such behavior was also observed in [17]. As the amount of ruthenium on the cathode catalyst increases, the peak sizes become similar. Surface morphology changes lead to more uniform structure and the peaks due to Ru and Pt merge.

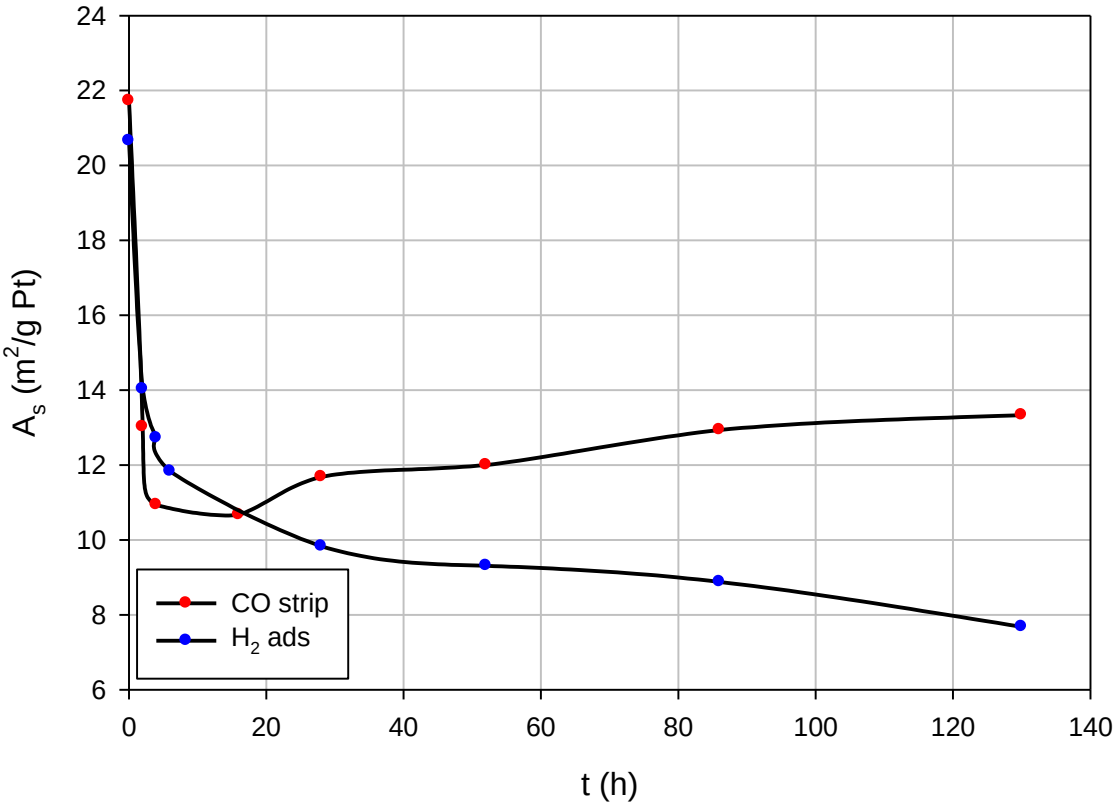

Figure 20. Specific active area (A_s) change in time during anode polarization experiment. Comparison of results obtained from charge integration in CO stripping (CO strip) and hydrogen adsorption (H_2 ads).

The active surface area of the cathode calculated from CO stripping charge and hydrogen adsorption charge show significant initial degradation by almost 25% in only the few first hours of the current-less ruthenium crossover experiment. During the current-assisted ruthenium crossover experiment, the active surface area based on the CO stripping charge initially decreases and then starts to increase with increasing ruthenium content deposited on the platinum catalyst. The specific surface area of cathode catalyst is roughly the same before and after the anode polarization experiment. The changes in the cathode active surface area during the experiment are an effect of changing surface structure resulting from rearrangement and changes in oxidation state of the deposited ruthenium. The lack of

overall change in active surface area of the cathode catalyst due to ruthenium deposition was also reported in [11], but intermediate states of active surface area were not described.

The surface area determined from hydrogen adsorption charge decreases continually. This is a result of a decrease in the amount of hydrogen adsorbed on platinum sites caused by ruthenium. The difference between the active surface area, calculated on the basis of CO stripping charge and H_2 adsorption charge, increases with increased amount of deposited ruthenium. The hydrogen adsorption charge integration, successful in the active surface area determination for platinum, cannot be used for a ruthenium-contaminated catalyst. For ruthenium, it has been previously reported that the hydrogen desorption charge does not correlate well to the expected surface area due to interferences from ruthenium hydroxides [18]. The CO stripping method gave accurate results for PtRu catalysts when compared to the BET surface area [19].

8.4 XRF catalyst characterization

Ruthenium content in the cathode catalyst after the anode polarization experiment was quantified using XRF technique. The results are presented in Table 6.

Table 6. XRF measurements for anode and cathode catalyst loading and weight fraction in the tested MEA for DMFC after the anode polarization experiment.

Electrode	cathode	anode
loading [mg catalyst/cm^2]	2.978	4.906
platinum [wt%]	97.14±1.128	64.35±0.642
ruthenium [wt%]	2.86±0.077	35.65±0.188

As shown in Table 6, the weight percentage of Ru in the cathode catalyst has increased and reaches nearly 3 wt%, indicating severe ruthenium contamination. The anode catalyst does not show significant changes in composition. It is in good accordance with the CO stripping voltammetry results for the anode catalyst, where the peak potential does not show a noticeable shift to the more positive potential region. This means that the ratio of platinum to ruthenium on the anode surface remains unchanged. Both anode and cathode catalysts show slightly decreased loading compared to the XRF results for the initial half-MEAs. This may result from the catalyst movement into the membrane during fuel cell operation, as previously observed by Shao-Horn *et al* and Borup *et al.*

9 CATHODE PERFORMANCE LOSS DUE TO RUTHENIUM PRESENCE

In the anode potential hold experiment the cathode catalyst was severely contaminated with ruthenium. In this section, fuel cell performance with the degraded cathode will be compared to the initial performance in order to quantify the contamination impact.

9.1 Experimental

Cathode performance degradation resulting from ruthenium crossover was evaluated from cathode polarization curves. Such curves can be calculated from the data obtained from i-R corrected measurements of voltage vs. current density (j-V) for the following cell operation modes:

- methanol-air, where the anode is supplied with 0.5 M methanol and the cathode is supplied with air,
- methanol-hydrogen, driven by an external power source, where the anode is supplied with 0.5 M methanol and the cathode, supplied with hydrogen, acts as a hydrogen evolving electrode (HE),
- 'hydrogen pump', driven by an external power source, where both the anode and the cathode are supplied with hydrogen; one of the electrodes acts as a hydrogen evolving electrode (HE) and one of the electrodes serves as a hydrogen oxidizing electrode (HO).

The test conditions were kept consistent with the initial tests described in Chapter 7 to assure valid comparison: cell temperature 80^{o}C, air humidification temperature 90^{o}C, air backpressure 20 psig, air-flow rate 500 sccm, hydrogen humidification temperature 90^{o}C, hydrogen backpressure 20 psig, and hydrogen flow rate 200 sccm.

The experimental data provided information about potential differences as a function of current density in each operation mode. They can be described mathematically, by using Equations 6, 7, 8:

$$V_{MEOH-air}(j) = E_{air}(j) - E_{MEOH}(j) \quad (6)$$

$$V_{MEOH-H2}(j) = E_{MEOH}(j) - E_{HE}(j) \quad (7)$$

$$V_{HE-HO}(j) = E_{HO}(j) - E_{HE}(j) \quad (8)$$

where:

$E_{air}(j)$ – air cathode potential in DMFC operation conditions,

$E_{MEOH}(j)$ – methanol anode potential,

$E_{HO}(j)$ – hydrogen oxidizing electrode potential,

$E_{HE}(j)$ – hydrogen evolving electrode potential.

The cathode potential versus a hydrogen oxidizing electrode, derived using Equations 6, 7, 8, was calculated with the use of Equation 9.

$$E_{air}(j) - E_{HO}(j) = V_{MEOH-air}(j) + V_{MEOH-H2}(j) - V_{HO-HE}(j) \qquad (9)$$

In order to complete the cathode performance analysis, the influence of methanol crossover on 'ruthenium free' and severely ruthenium contaminated cathode will be discussed with respect to these additional studies. The cathode performance loss due to methanol crossover can be quantified by the difference between the iR-corrected, hydrogen-air polarization curve and the calculated cathode potential as a function of current density for the methanol-air operation mode.

9.2 Results and discussion

Not iR-corrected polarization curves in methanol-air operation mode for the cells with the 'ruthenium-free' and the severely ruthenium-contaminated cathode are shown in Figure 21. The term 'ruthenium-free' refers to a fuel cell that only suffered an unavoidable ruthenium contamination, occurring during humidification and "break-in". Although not truly "Ru-free", the degree of contamination is much smaller in this case compared to that obtained after the anode polarization experiment.

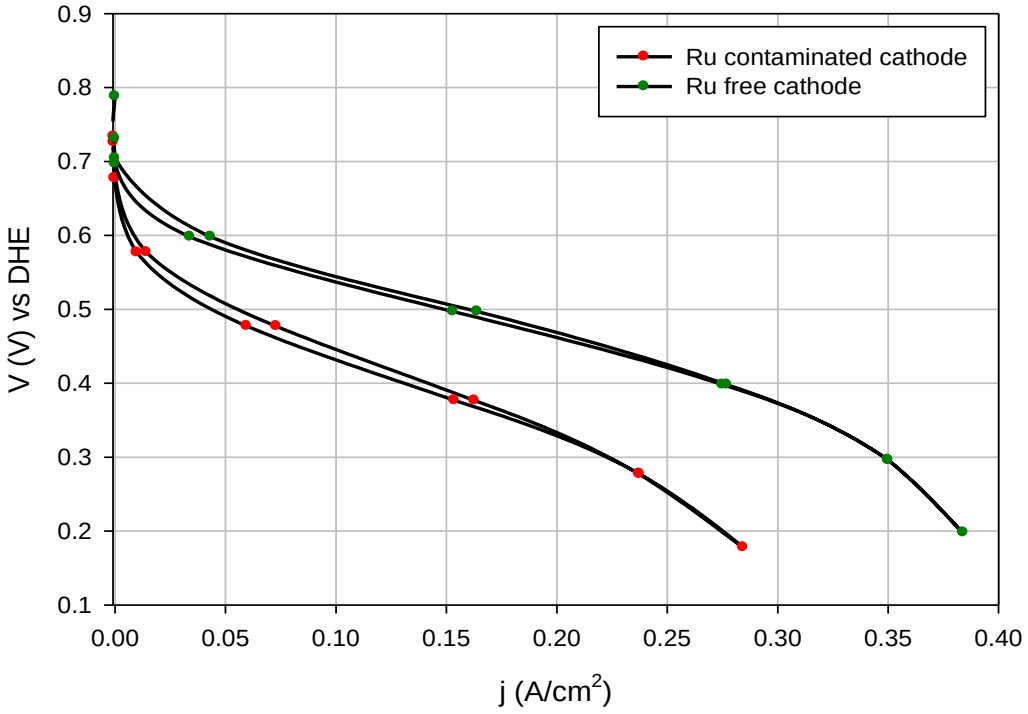

Figure 21. Polarization curves for the same cell supplied with 0.5 M methanol and air oxidant with ruthenium-free and ruthenium-contaminated cathode.

There is very large performance degradation due to ruthenium crossover and its deposition on the cathode, which results in decreased ORR kinetics. At the standard potential of 0.5 V the cell reaches the current density of 0.05 A/cm^2 instead of 0.15 A/cm^2 obtained before the anode potential-hold experiment was performed. The cell shows a relative performance degradation of 66% at 0.5 V. The high frequency resistance of the cell does not change due to anode polarization experiment, which indicates that the performance degradation cause is only the catalyst degradation and there are no other factors influencing the results.

The plot of cathode potential versus current density together with the results obtained from anodic polarization, cell polarization and hydrogen-pump experiment ruthenium are shown in Figure 22 for the 'ruthenium-free' and severely ruthenium-contaminated cathode.

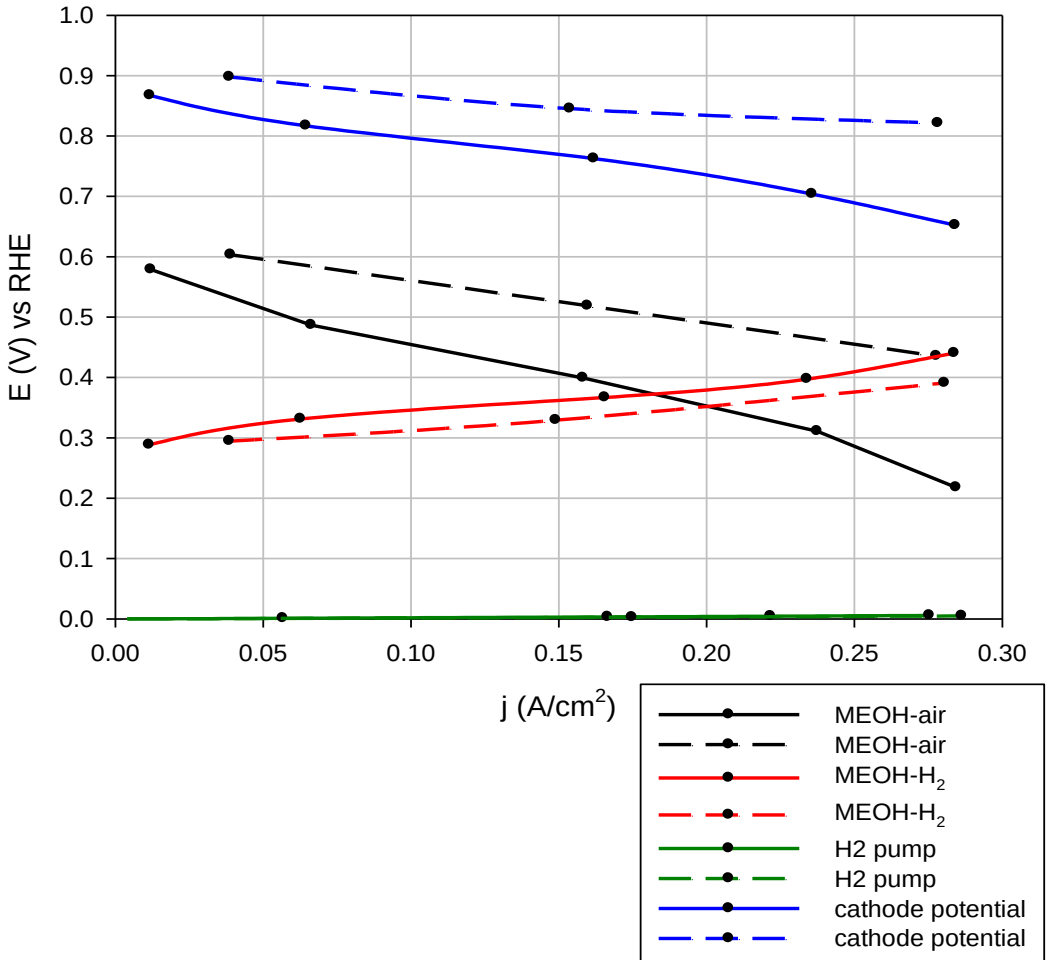

Figure 22. Cathode potential plot for DMFC cell with ruthenium-free (dashed line) and ruthenium-contaminated (solid line) cathode.

According to Figure 22, the correction for the variation of the hydrogen oxidation potential with current density is negligible and is not affected by the anode polarization experiment. Moreover, Figure 22 shows that the anode polarization experiment only slightly affected the anode activity. After the experiment, the anode potential is on average 20 mV higher

than for an initial MEA. This is a result of loss of ruthenium from the anode which decreases the methanol oxidation kinetics. The cathode potential loss due to ruthenium poisoning is equal to 80 mV for low current densities and increases to 120 mV for high current densities. The obtained results show significant similarities to the results obtained in [8], but because test conditions are different in both cases a direct comparison of the data cannot be made.

The comparison of cathode performance loss due to methanol crossover is shown in Figure 23. These losses were determined from the difference between the iR-corrected hydrogen-air cell polarization curves and the cathode polarization curves for 'ruthenium-free' and severely ruthenium-contaminated cathode.

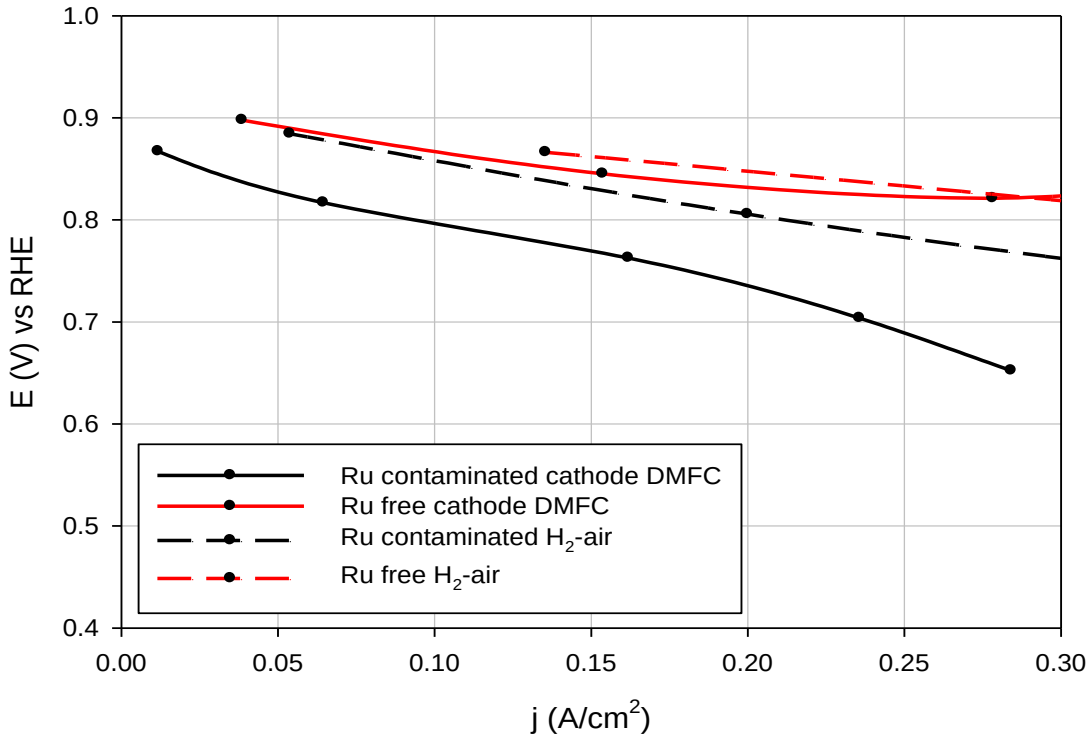

Figure 23. The effect of methanol crossover on cathode potential.

Knowing the driving force and the principles of methanol crossover mechanism described in Chapter 2, it no surprise to observe decreasing amount of methanol on the cathode with increasing current density. At the limiting current density, when the entire methanol is being consumed at the anode, the methanol crossover becomes zero. Figure 23 shows that for a MEA with an uncontaminated cathode, methanol crossover becomes negligibly small for current densities higher than 0.28 A/cm^2.

The results for a cell after the anode potential hold experiment (severely contaminated cathode) are not in accordance with this theory and are difficult to interpret. The cathode polarization curves obtained in hydrogen-air operation mode and methanol air operation mode do not meet at any point. This means that, except for methanol crossover, there is

another source of performance loss in methanol-air operation mode or that some additional degradation appeared in between the two polarization curves were taken. Results for 'ruthenium-free' cathode shown in Figure 23 show similarities to the results presented in [8] but are not directly comparable, due to different testing conditions.

10 ORR DEGRADATION DUE TO RUTHENIUM PRESENCE AT THE CATHODE-RDE EXPERIMENT

It was shown in Chapter 9 that ruthenium crossover causes a decrease in cathode catalyst activity in oxygen reduction reaction, which is a main cause of the overall performance loss. The effect of ruthenium presence at the cathode on ORR was further investigated with the use of a rotating disc electrode in order to find a relation between the amount of deposited ruthenium and its impact on ORR kinetics.

10.1 ORR mechanism

The oxygen reduction reaction is known to be sluggish and is characterized by substantial overpotential. Improving the kinetics of this reaction in acidic media is a problem of great importance and has been extensively studied.

As described in [20], after being transported by diffusion to the electrode molecular oxygen undergoes a complex multistep process of electrochemical reduction. The mechanism of this process is illustrated in Figure 24.

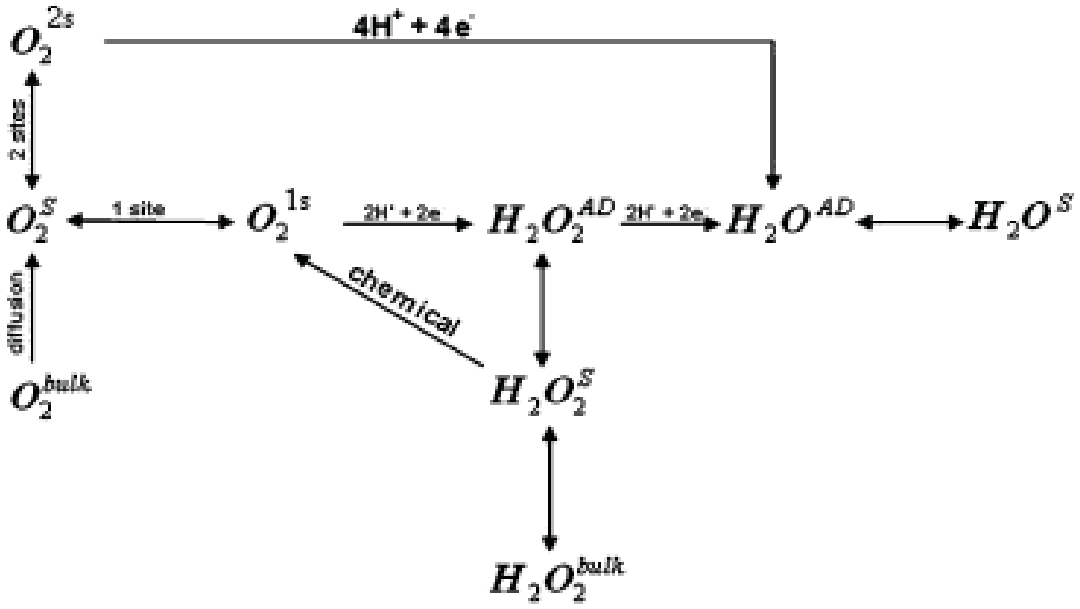

Figure 24. Schematic of mechanism of oxygen reduction reaction in acidic media [20].

The reaction can result either in water or peroxide formation depending on the ORR catalyst used and also type of oxygen adsorption. When the reaction proceeds via two-site adsorption process on platinum the four electron reduction process occurs and water molecule is formed. In case of a single-site adsorption on platinum, the dual bond is rearranged and the product is peroxide.

Catalysts show different activity in reducing oxygen. Platinum is considered to be the absolute leader of pure elements in activity for electrochemical reduction of oxygen in acidic media. The Tafel slope in low overpotential region and high coverage was reported to be 60 mV/dec and 120 mV/dec in high overpotential region and low coverage, respectively [21].

10.2 RDE basics

The rotating disc electrode (RDE) experiment is a hydrodynamic method of electrochemical characterization of reactions. The electrode rotates in the solution which causes increased mass transport of the reactants due to forced convection. Hydrodynamic methods have many advantages. The convection-limited mass transport provides higher current densities than steady-state diffusion-limited mass transport conditions can provide. The relative mass transport influence on reaction kinetics is not significant. In RDE experiments the rate of mass transport is easy to control by changing rotation speed. It ensures obtaining repeatable mass transport conditions. The RDE experiment is commonly used to characterize fuel cell catalyst activity for the oxygen reduction reaction (ORR) or hydrogen oxidation reaction (HOR).

Important for the RDE experiment is the limiting current, which represents maximum reaction rate under certain conditions (speed of rotation, viscosity, diffusivity, and reactant concentration). The limiting current is reached when the concentration of reactants on the surface is equal to zero, which means that the reaction rate cannot be further increased without an increase of reactants supply, ie by an increase of concentration or rotation speed. This current for a RDE is described by Levich equation:

$$i_L = 0.62nFAD_o^{2/3}\omega^{1/2}\vartheta^{-1/6}C_o^*$$

where:

n– number of electrons in the reaction

F– Faraday constant

A– Geometric surface area

D_o– diffusivity [m^2/s]

ω – rotation speed [rad/s]

ϑ– kinematic viscosity

C_o^*– concentration of reactants.

The limiting current value is, however, dependent on many factors. It decreases linearly with decreasing ambient pressure, so a correction factor is required for the Los Alamos altitude. It is also dependent on the temperature at which the experiment is performed.

The second important parameter which characterizes the catalyst activity in ORR is the half-wave potential, which is the potential at which half of the limiting current is reached.

The RDE experiment results are affected by adsoption processes and the ohmic drop caused by system resistance, so it is important to make a correction for those effects. The underpotentially-deposited hydrogen and oxide formation processes result in current flow which superimposes on the ORR curve. The ohmic drop affects the mass-transport influenced region of i-V curve and the Tafel slope might contain a significant error due to that effect [22]. The ohmic drop can be determined by high frequency resistance measurements under the operating conditions. The resistance is dependent on current and solution concentration according to [22]. The solution resistance is also dependent on temperature and it decreases with temperature increase.

10.3 ORR at platinum RDE

10.3.1 Experimental

Before the oxygen reduction was performed on the platinum disc, a collection efficiency of the ring was experimentally verified with the use of the ferricyanide experiment. (see Appendix A for details).

Before performing ruthenium deposition, the characteristics of the pure platinum disc electrode were determined. Platinum disc was used to obtain cyclic voltammetry in oxygen-free electrolyte, polarization RDE curves in oxygen-saturated solution, and CO stripping voltammetry. The experiments were performed in a three-electrode cell. The electrolyte used was 0.1 M perchloric acid ($HClO_4$). The potential was measured versus RHE (platinized platinum wire and 6% $H_2|N_2$). The counter electrode used was a platinized platinum wire. The reference and counter electrodes were separated from the main compartment with a frit in order to avoid contamination by ruthenium. The experiments were performed with the use of CH Instruments 750B potentiostat and a Pine rotator. The rotating ring-disc electrode used was of the E7R8 series, manufactured by Pine Instruments, with the disc area of 0.1642 cm^2. A three-compartment electrochemical cell experimental setup is shown in Figure 25.

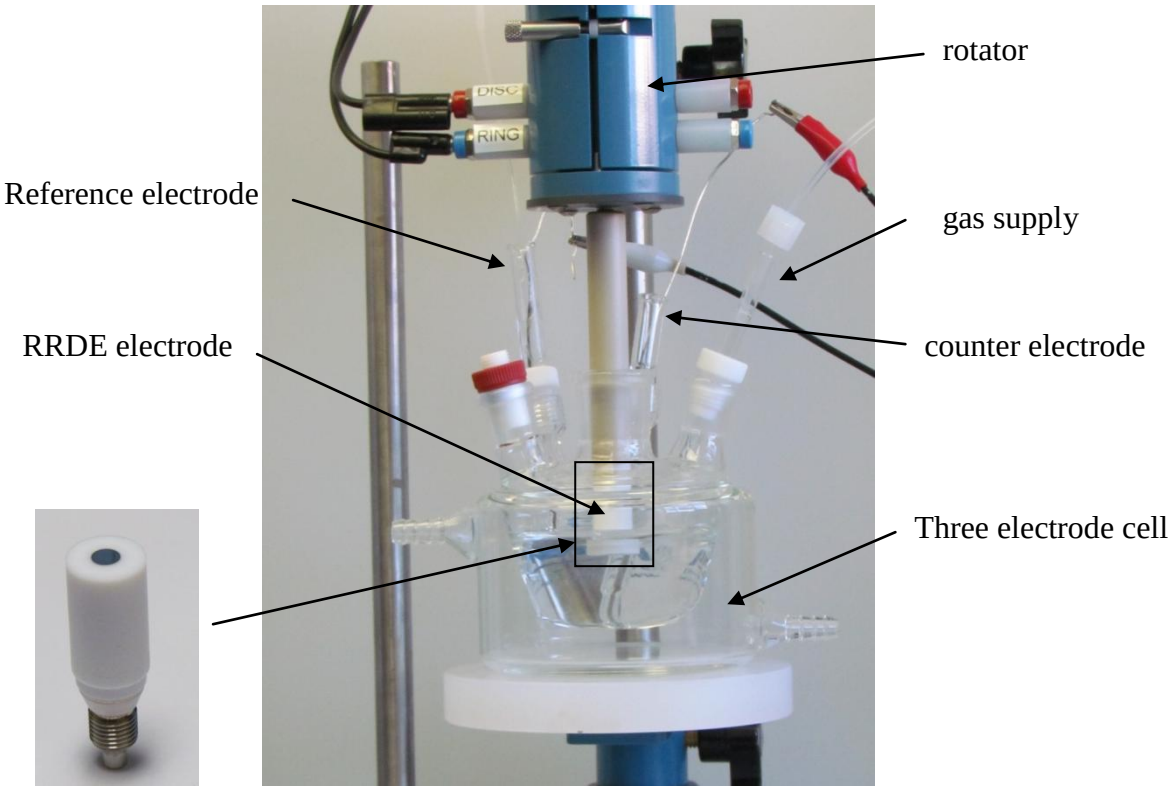

Figure 25. RRDE experimental set-up for the determination of ruthenium impact on ORR kinetics.

Cyclic voltammetry at a scan rate of 200 mV/sec was performed under nitrogen atmosphere which was obtained by bubbling UHP nitrogen. The potential range was 0 V to 1.3 V vs forming gas, the potential range was chosen in a way so that the cycling mimics the cycling being done in a fuel cell during the anode polarization experiment. To account for the difference between 6% $H_2|N_2$ and 100% H_2 a correction by 40 mV was performed to refer potentials to the RHE reference electrode.

The cyclic voltammetry was followed by the CO stripping experiment. The cell was already under nitrogen atmosphere, so initial nitrogen purging was not required. 9.97% CO in ultra high purity (UHP) nitrogen was bubbled and CO was adsorbed for 10 min at a potential of 0.1 V vs. RHE. After the adsorption process was completed, the cell was purged with N_2 in order to remove non-adsorbed CO from the solution for 10 min. The CO stripping voltammetry was performed at a scan rate of 5 mV/sec, in the potential range of 0 to 1 V. The potential range was narrowed in order to avoid ruthenium dissolution due to exposure to high potential. The CO stripping procedure was the same for all the experiments performed. The CO stripping peak potential is highly dependent on the nitrogen purging time after the CO adsorption and the gas flow rates. The CO coverage never reached 100%. There were always platinum sites with adsorbed OH groups. The degree of coverage reached by CO is highly sensitive to experimental conditions, so these conditions must be kept consistent if results are to be compared.

The CO stripping characterization was followed by oxygen reduction reaction using ultra high purity (UHP) oxygen bubbled though the solution to ensure saturation. The ORR currents were measured for rotation speeds of 400 rpm, 900 rpm, 1600 rpm and 2500 rpm at a scan rate of 20 mV/sec. The values of limiting current were corrected for Los Alamos altitude and are given below for the pressure of 1 atm and the temperature of 25^{o}C.

10.3.2 Results and discussion

The ring collection efficiency values determined using the ferricyanide experiment at different rotation speeds are shown in Table 7.

Table 7. Collection efficiency of platinum disc electrode measured with a ferricyanide experiment.

rpm	efficiency [%]
400	24.2
900	23.7
1600	23.5
2500	23.3
3600	23.0

The collection efficiency varies slightly for different rotation speeds due to slight differences in the hydrodynamics. The results are in good agreement with specifications provided by the producer which state that the collection efficiency is 22%.

The results of cyclic voltammetry for platinum RDE in 0.1 M $HClO_4$ at 200 mV/sec scan rate are shown in Figure 26.

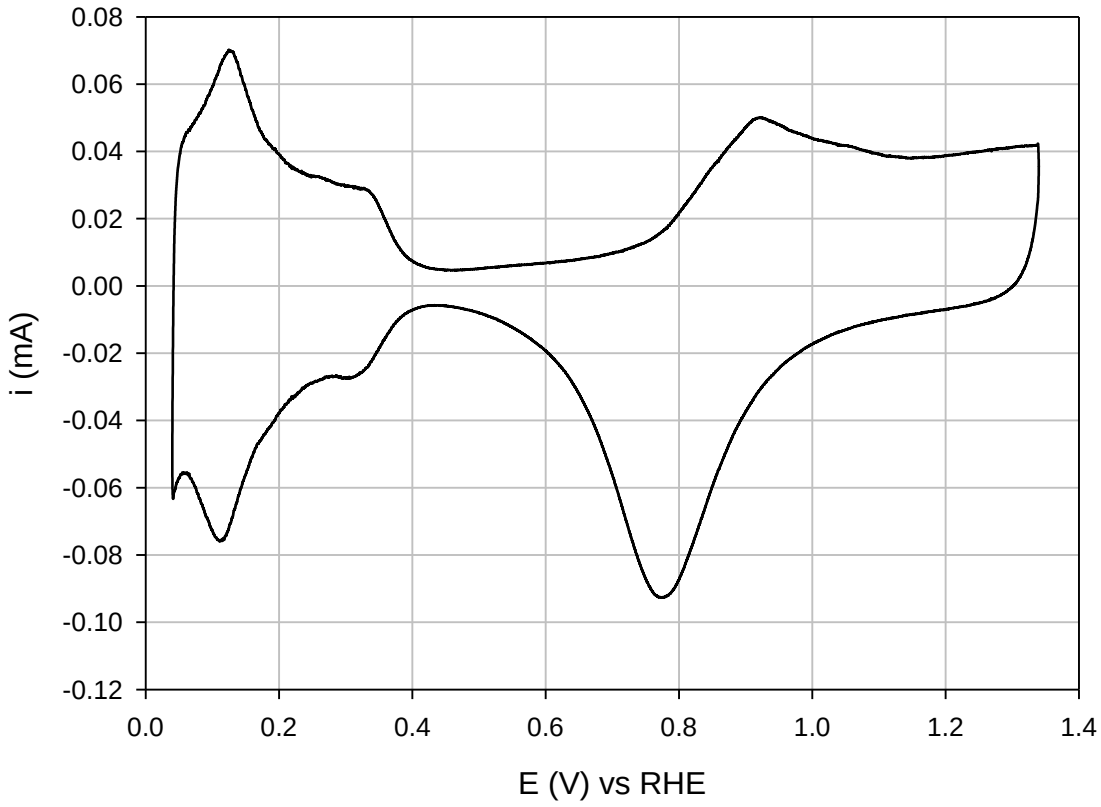

Figure 26. Cyclic voltammogram of platinum rotating disc electrode in 0.1 M $HClO_4$ at 200 mV/sec scan rate.

The results do not indicate any impurities and show all the characteristic features for platinum which are the following: hydrogen adsorption, oxides formation, oxide reduction, and hydrogen evolution.

The results of CO stripping voltammetry for platinum RDE at a scan rate of 5 mV/sec are shown in Figure 27.

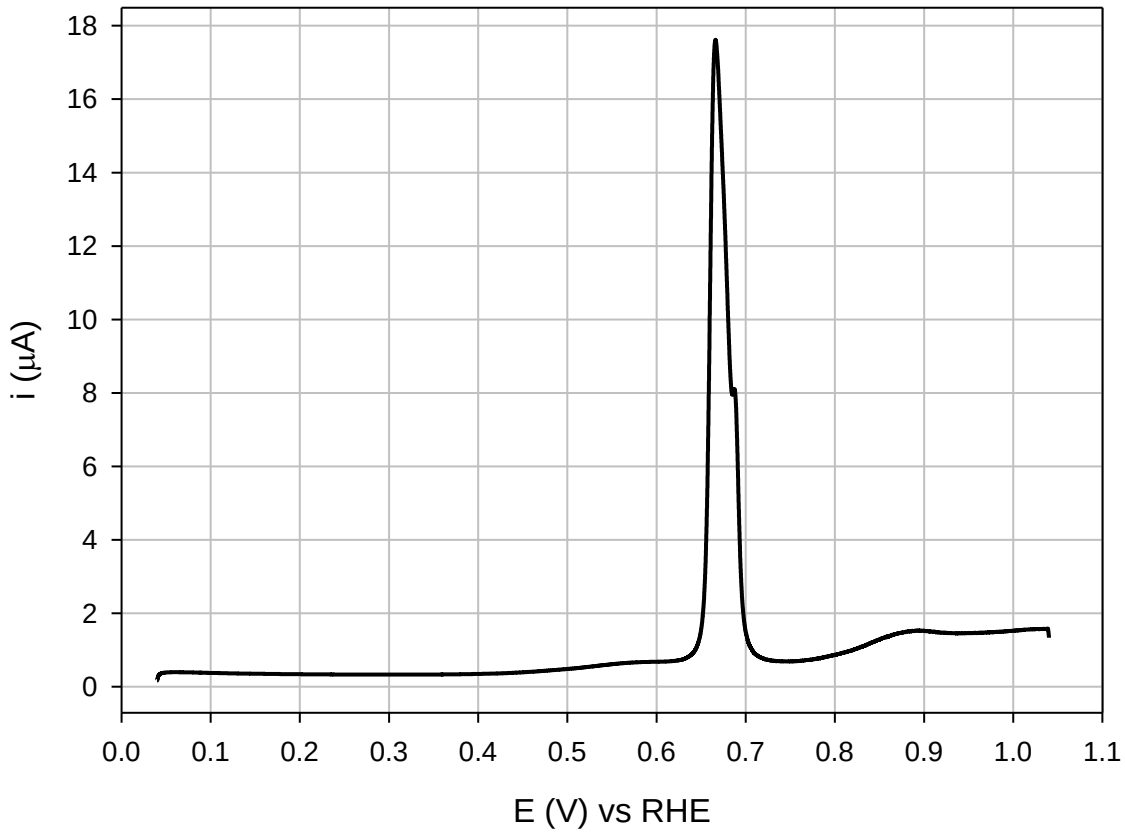

Figure 27. CO striping voltammetry for platinum rotating disc electrode.

The CO stripping peak potential is 0.67 V vs. RHE, in agreement with [11]. The peak is very sharp which means that CO forms a homogeneous type of bonding with platinum of equal binding energy.

The oxygen reduction reaction current transients for rotation speeds of 400 rpm, 900 rpm, 1600 rpm and 2500 rpm at the scan rate of 20 mV/sec are shown in Figure 28.

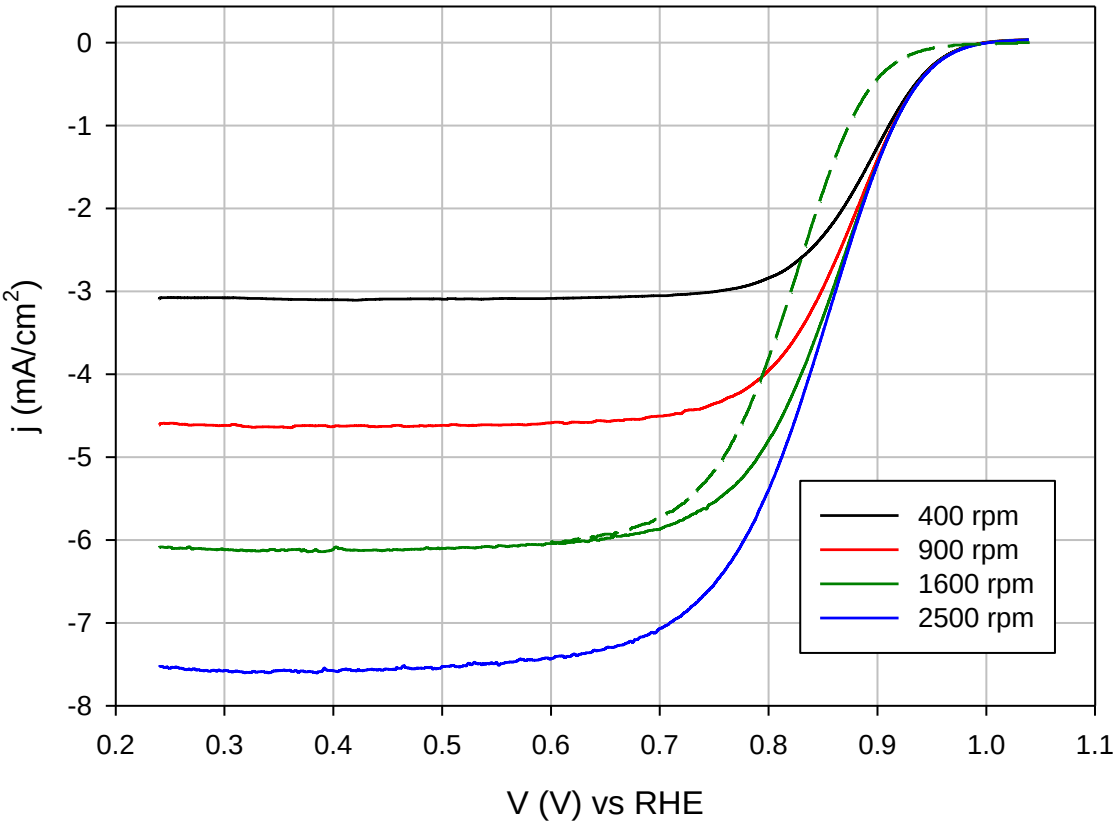

Figure 28. Oxygen reduction reaction at a platinum RDE: cathodic (dashed line) and anodic (solid line) sweeps recorded at 400 rpm, 900 rpm, 1600 rpm, and 2500 rpm; scan rate 20 mV/s.

The limiting current density values, reached for every rotation speed, are in good accordance with literature [23]. The half-wave potential is 0.84 V vs. RHE. The results shown in Figure 28 are iR-corrected.

10.4 ORR on ruthenium-contaminated platinum RDE

After measuring the characteristics of an unmodified Pt disc, Ru deposition experiment was carried out. Ruthenium was deposited on the platinum disc using spontaneous deposition method [24]. This method was chosen because it is simple and does not require the use of electrochemical instruments. The ORR performance of the ruthenium-contaminated electrode was compared with the previously determined performance of the pure platinum disc.

10.4.1 Experimental

Ruthenium deposition was performed by providing a drop of solution containing ruthenium ions on the platinum disc very carefully, so that the ring did not become contaminated. The solution from which ruthenium was deposited was 1 mM hydrated Ru(III) chloride ($RuCl_3 \cdot xH_2O$) in 0.1 M perchloric acid ($HClO_4$).

The deposition was performed for three different depositing times: 10 sec, 1 min and 5 min. After deposition the ruthenium-containing solution drop was rinsed from the disc with Millipore 18.2 MΩ water. The electrode was dipped in the electrolyte solution and testing was executed. After each deposition and before performing tests, a cyclic voltammogram was obtained in the potential range 0.0 V-1.0 V vs. a forming gas reference. The purpose was to ensure reduction of ruthenium oxides formed on the surface and to reach a stable surface state. The upper potential limit for CV, CO stripping voltammetry and ORR experiments was chosen to be 1.0 V vs. a forming gas reference electrode in order to prevent ruthenium dissolution from the disc surface due to high potential exposure. After each experiment a cyclic voltammogram was performed in the potential range 0.0 V-1.3 V vs. a forming gas reference electrode in order to remove ruthenium from the platinum disc surface.

10.4.2 Results and discussion

The change of properties of catalyst due to ruthenium presence depends on the amount of this element and surface morphology. Ideally, the amount of ruthenium should be quantified with the use of STM measurements, which is beyond the scope of this study, but was done for several conditions also used in this work [24], so the ruthenium coverage was estimated on the basis of available in the literature data. It was discovered that ruthenium coverage on platinum surface depends on the crystal structure of platinum. After 2 min of spontaneous deposition from 1mM $RuCl_3$ in 0.1 M $HClO_4$, a coverage of 0.18 ML, 0.09 ML and 0.21 ML for Pt(111), Pt(110) and Pt(100), respectively, was reported in [17]. It was reported in [24] that a single spontaneous Ru deposition yields ruthenium in the form of nano-islands and the saturation coverage of 0.2 ML cannot be exceeded on Pt(111). The coverage can be increased by performing additional depositions from a ruthenium containing solution followed by reduction of ruthenium oxides. A second spontaneous deposition of ruthenium on Pt(111) increases the coverage from 0.18 ML to 0.22 ML for Pt(111) [24]. It was discovered that ruthenium islands increase in height after repeated depositions, which leads to a conclusion that ruthenium preferentially deposits on the ruthenium surface. It was reported in [24] that the morphology of deposited ruthenium changes with electrode potential change. At a potential of 0.1 V vs. Ag|AgCl, ruthenium is present in a metallic state. An increase in potential to 0.35 V vs. Ag|AgCl was found to cause ruthenium oxides formation and an increase in the size and height of ruthenium islands. A further potential increase up to 0.7 V vs. Ag|AgCl caused ruthenium islands disintegration. Sweeping the potential back to 0.1 V, caused reduction of ruthenium oxides and was found to result in higher ruthenium dispersion and reduction in the size of ruthenium islands relative to that obtained after the deposition and before potential

sweeping. Due to a higher dispersion of ruthenium atoms the coverage was found to increase from 0.22 ML to 0.25 ML after potential cycling and thus the amount of platinum sites available for chemisorption on the PtRu surface decreased.

The changes of ruthenium content on platinum disc electrode were determined with CO stripping experiment. The results of CO stripping voltammetry which was performed after each deposition are shown in Figure 29a and respective CV scans which followed CO stripping are shown in Figure 29b.

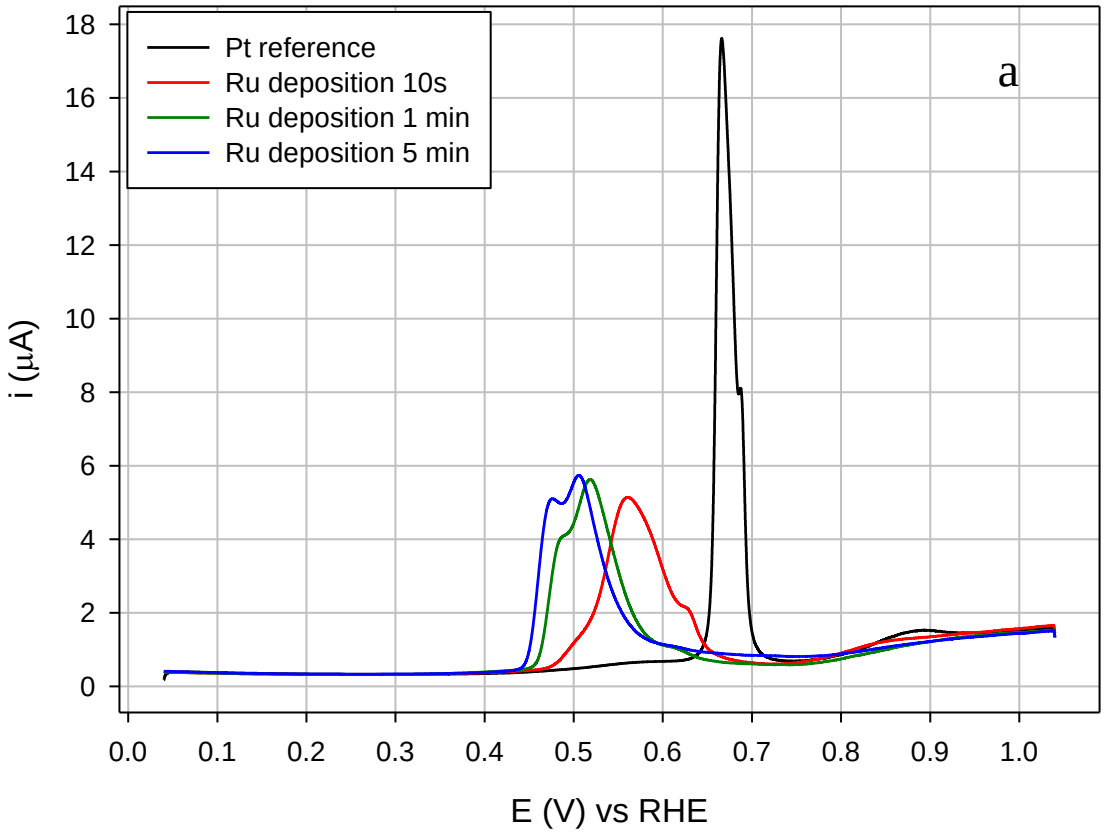

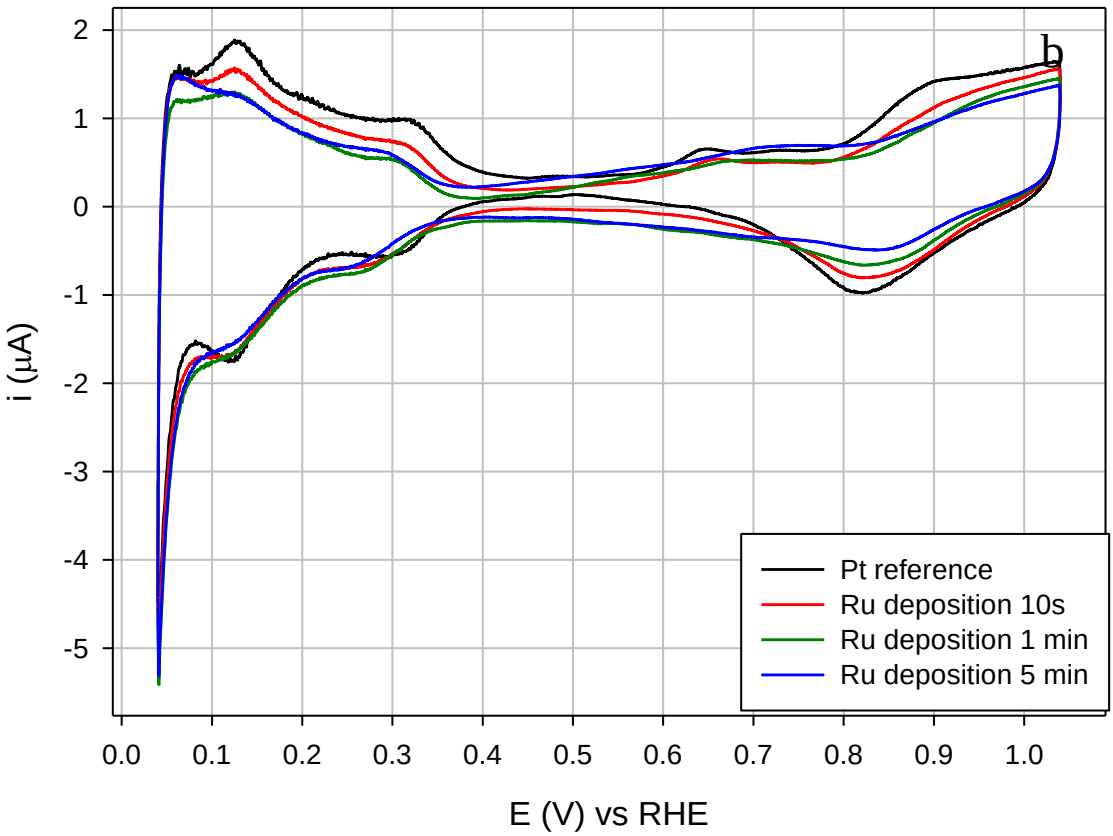

Figure 29. CO stripping voltammetry: (a) CO stripping peaks, (b) CO-free CVs for platinum RDE and different times of ruthenium spontaneous deposition.

According to Figure 29a after only ten seconds of spontaneous deposition, there is a significant negative shift of the CO stripping peak potential. It is also visible that the peak is wide and splits into the main peak and a little peak in higher potential region. When the deposition time increases, the CO stripping peak potential shifts negatively and the two split peaks become similar in size. Splitting of the CO stripping peak into two was investigated in [17] and [24]. It results from the oxidation of CO on Ru surface and on Pt near Ru islands at lower potentials and on the Pt surface at higher potential. The CO stripping peak potential and shape depend on Ru coverage and morphology which were proved to change during potential cycling.

The results of CO stripping experiments obtained for platinum disc electrode show great similarity to the results obtained for anode polarization experiment performed in a fuel cell. In the ruthenium spontaneous deposition experiment no final merge of Pt-related and Ru-related CO stripping peaks can be seen. More experiments at longer deposition times may be needed.

The plot that correlates the CO stripping peak potential with time is shown in Figure 30. The plot corresponds to the platinum-related part of the split CO stripping peak. The saturation coverage was reported in literature to be achieved within 3 min deposition [24].

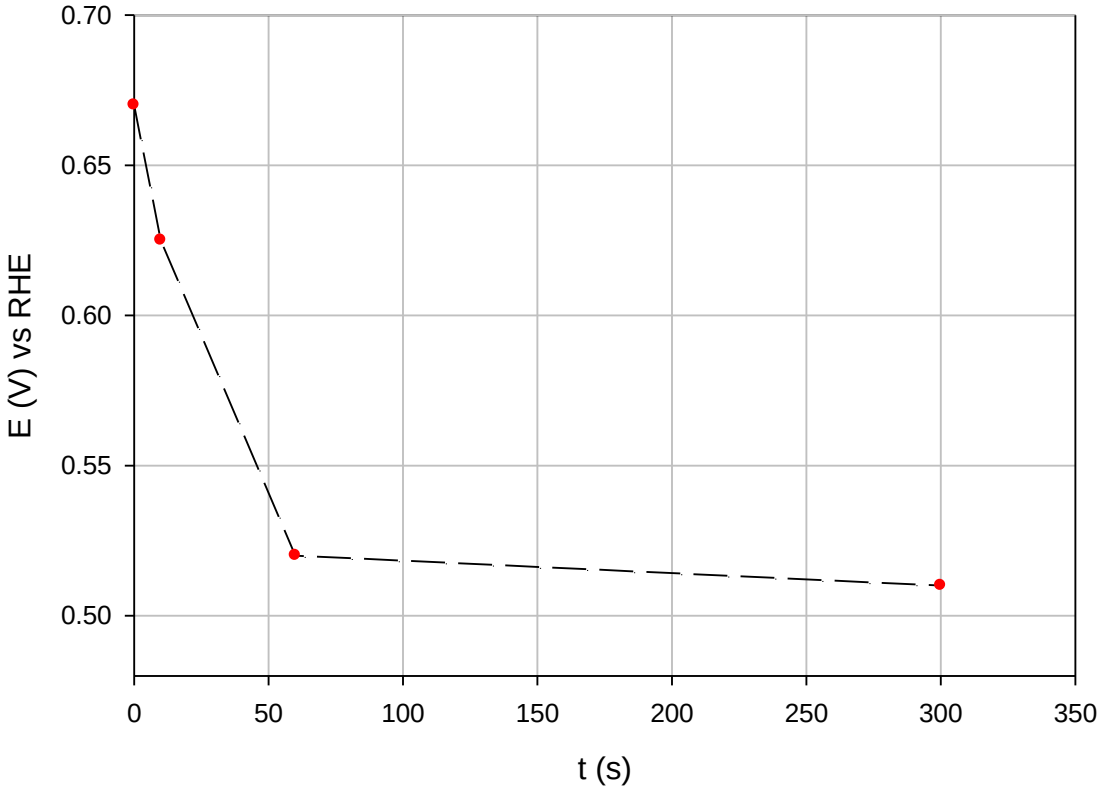

Figure 30. Shift of the CO stripping peak potential as a function of Ru deposition time at a platinum RDE.

As presented in Figure 30, the rate of contamination in the spontaneous deposition of ruthenium on platinum disc is similar to the one in the fuel cell anode potential hold experiment shown in Figure 19. In both cases the biggest potential shift occurs initially and longer deposition or prolonged potential hold cause more surface rearrangement reflected in the CO stripping peak shape than in the potential shift. In case of the platinum disc ruthenium contamination only four data points were obtained and this data may not show the full picture of the contamination process. Despite indicated similarities with the fuel cell contamination process, the timescales for the two experiments are different.

Future work might result in confirming the correlation, which would enable predicting fuel cell behavior based on RDE results. To date, the results are promising and can contribute to developing new methods of mitigating or reducing the devastating effect ruthenium has on the platinum catalyst ORR activity.

The ORR voltammetry results presented in Figure 31 were corrected for the Ohmic resistance losses which otherwise can significantly influence the Tafel slope and half-wave potentials [22]. The electrolyte resistance, determined from HFR measurements, is

dependent on temperature, and electrolyte concentration. The electrolyte used in this study (0.1 M $HClO_4$) ensured a constant ohmic drop during the experiment. The resistance value was not measured during experiments and the correction was made on the basis of [22] which reports 28.5 Ωcm for 0.1 M $HClO_4$ electrolyte at 293K. The average error due to resistance was calculated to be 4%. However, the error in the diffusion-limited current region was higher, at 10%.

The second source of error in oxygen reduction experiments results, accounted for in this study, is related to the presence of the double-layer capacitive current. This effect depends on the scan rate used and decreases when the scan rate is lowered. However, platinum is very sensitive to impurities and very low scan rates are not preferable. The contribution of capacitive currents is a function of surface area and was reported in [22] to vary from 0.6% for Pt(111) up to 30-50% for high surface area Pt nanoparticles. In this study, the average influence of capacitive currents was calculated to be 0.7%.

The ORR kinetics after each ruthenium deposition time and for a platinum reference RDE at 1600 rpm rotation rate for the anodic sweeps corrected for the Ohmic resistance losses and capacitive currents are shown in Figure 31.

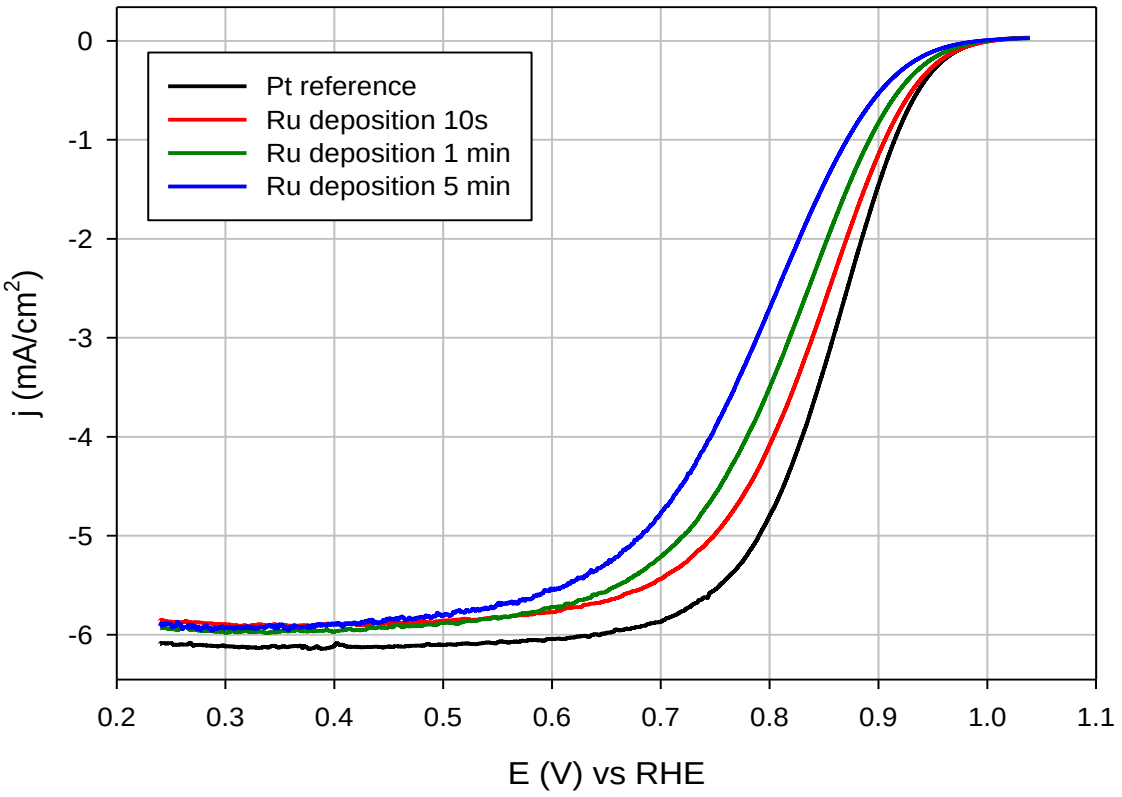

Figure 31. ORR at a platinum RDE following Ru deposition for different times; 1600 rpm, scan rate 20 mV/sec, 0.1 M $HClO_4$.

It can be seen that the half-wave potential shifts in the direction of lower potentials with increasing ruthenium deposition time. The ORR kinetics become slower and diffusion

limited current density is reached at a lower potential. The half-wave potential plot vs. Ru deposition time is shown in Figure 32.

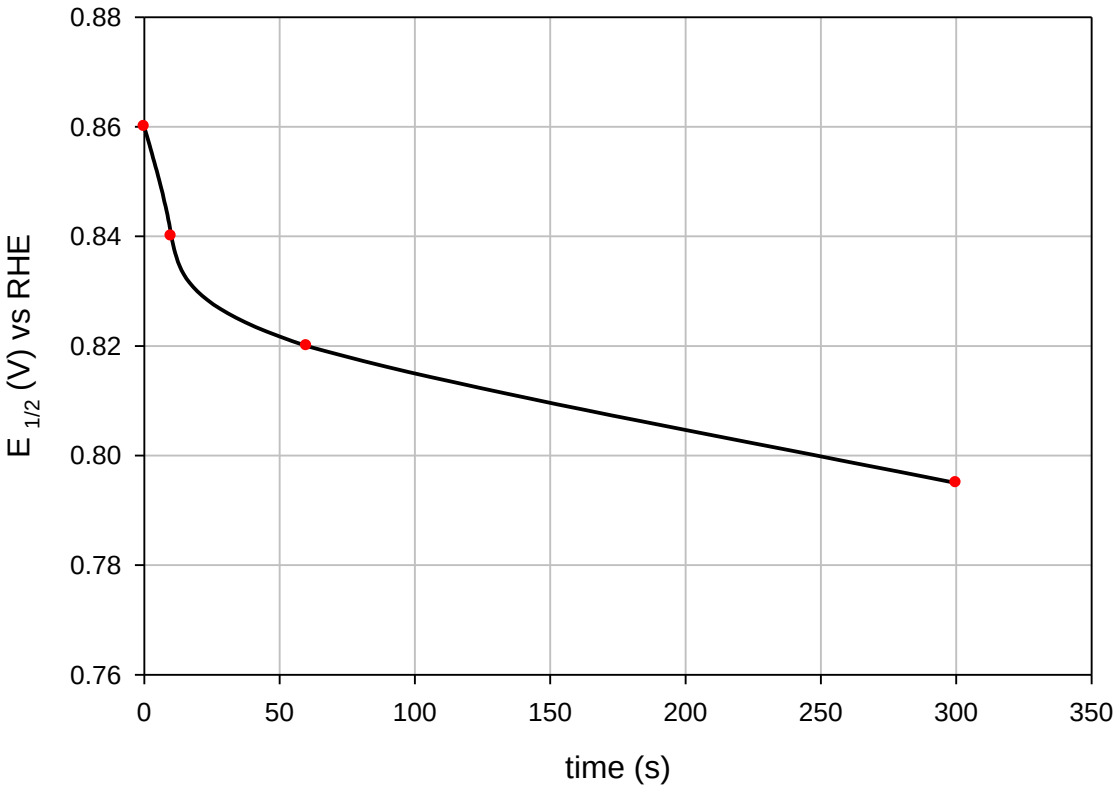

Figure 32. Half-wave potential of oxygen reduction reaction ($E_{1/2}$) as a function of time of ruthenium spontaneous deposition at a platinum RDE.

Figure 32 shows that the rate of half-wave potential shift in the direction of lower potential shows similarities with the CO stripping peak shift rate. However, unlike CO stripping peak potential, the half-wave potential of the ORR has not reached a minimum in the presented experiments. Its behavior at longer ruthenium spontaneous deposition times should be investigated. The oxygen reduction reaction kinetics is characterized by the Tafel slope, which represents the overpotential required to increase the rate of an electrochemical reaction by one order of magnitude.

The Tafel-slope comparison for ORR at pure platinum and Ru-contaminated platinum RDE is shown in Figure 33. The respective values of Tafel slope are given in Table 8.

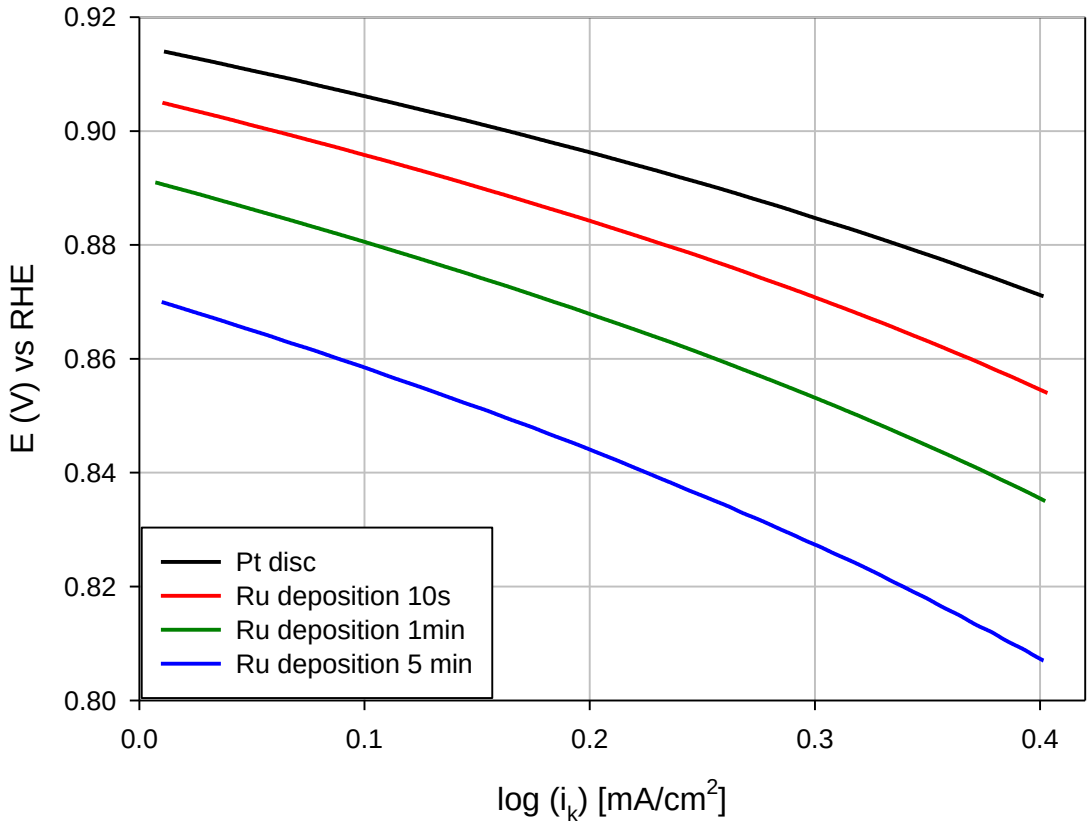

Figure 33. Tafel plots for ORR at an uncontaminated platinum disc (black line), and after spontaneous deposition of Ru for 10 seconds (red line), 1 min (green line), and 5 min (blue line).

Table 8. Tafel slope values (mV/dec) for ORR at pure and Ru-contaminated platinum RDE in 0.1 M $HClO_4$ (1600 rpm, 20 mV/sec scan rate)

	ruthenium deposition time (s)			
current density range (mA/cm^2)	0	10	60	300
0.01-0.1	86	103	113	128
0.1-0.2	98	116	127	143
0.2-0.3	125	135	147	167

The Tafel slope value increases with time of ruthenium deposition, which indicates slowing of the reaction kinetics. Similarly to the half-wave potential, the Tafel slope does not reach a constant value, suggesting that another spontaneous deposition could further increase its value. As shown in Table 8, the Tafel slope value changes with the current range selected for the calculation. This is a direct consequence a non-linearity of the current-potential plots.

Each oxygen reduction experiment was followed by potential cycling under UHP nitrogen atmosphere in the potential range of 0.04 V-1.34 V vs. RHE at the scan rate of 200 mV/sec, intended to remove deposited ruthenium from the Pt disc surface. The results are presented in Figure 34.

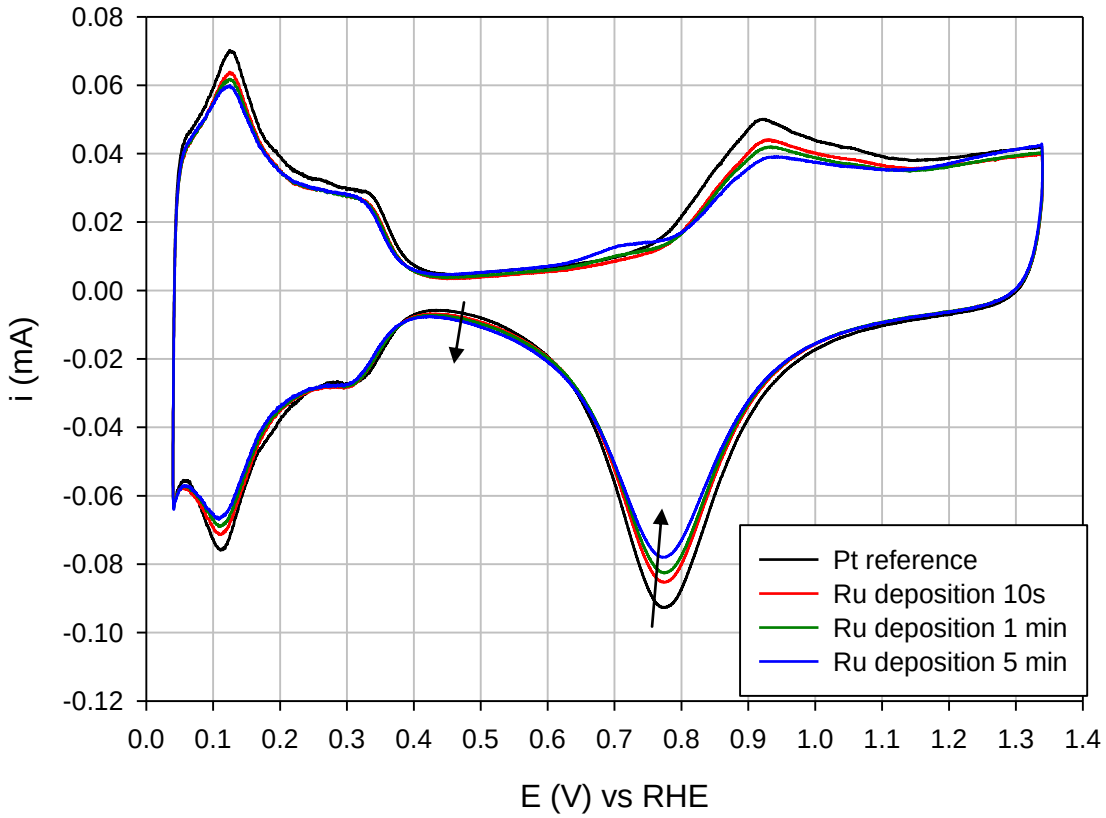

Figure 34. Potential cycling under nitrogen atmosphere after each spontaneous deposition of Ru (200mV/sec).

Cyclic voltammogram results obtained after each deposition do not overlap with results for platinum disc electrode, indicating that this potential range is not sufficiently wide to effectively remove ruthenium from the platinum disc. The changes characteristic of the ruthenium presence can be seen in the oxide reduction region and in the increased double-layer current (arrows). It is an important observation which can lead to explanation why a saturation coverage characteristic for a single spontaneous deposition is not reached (unlike in [24]). If ruthenium partly remains on the platinum disc surface, the multiple depositions performed lead to a higher ruthenium coverage and progressive oxygen reduction degradation. However, CO stripping voltammetry from a fuel cell anode shows that the ruthenium content reaches saturation and the CO stripping peak potential stabilizes at 0.49 V. This again leads to a conclusion that experiments involving more spontaneous depositions may be necessary for achieving saturation of the Pt disk surface with Ru.

11 RUTHENIUM CROSSOVER MITIGATION METHODS

As already discussed in this work, there are two main mechanisms for cathode contamination by ruthenium: current-less, which occurs after humidification without a current flow, and current-assisted, which takes place occurs during fuel cell operation. There is much ongoing work to enhance DMFC performance in terms of improving oxygen reduction kinetics as well as methanol oxidation. Different approaches to solving the Ru crossover problem have been explored by different research groups. The two main ones are the following: (1) removing dissolved ruthenium before deposition on the cathode, and (2) finding alternative catalysts which will demonstrate at least similar performance in methanol oxidation to that provided by the PtRu binary catalyst.

Ruthenium contamination appears already in the process of MEA preparation. It was noted in [11] that the MEA preparation method resulting in the lowest current-less contamination is a decal transfer of the anode and cathode catalysts onto two separate Nafion® 1135 membranes. The direct paining of catalysts inks on two membranes was reported to result in higher contamination [11]. The highest contamination was obtained when catalysts were transferred or directly painted on both sides of the same membrane [11].

The methods used for mitigating ruthenium contamination during MEA manufacturing are as follows:

- high-temperature-cured MEA approach,
- acid-pretreatment of the anode catalyst, where the anode catalyst is boiled in 0.5 M sulfuric acid,
- acid-pretreatment of the MEA (before cathode catalyst is applied), where the membrane and both catalysts are boiled separately in 0.5 M sulfuric acid,
- high-temperature MEA post-treatment *via* "decal transfer", which is based on hot pressing the MEA at 210^{o}C for 5 min.

Ruthenium contamination further increases during cell humidification. However, the most significant part of ruthenium contamination occurs during operation mode. One interesting ruthenium removal method was proposed by Yu Seung Kim, Jong-Ho Choi and Piotr Zelenay in a US patent nr 7,575,824 B2. A schematic diagram of the approach used is shown in Figure 35.

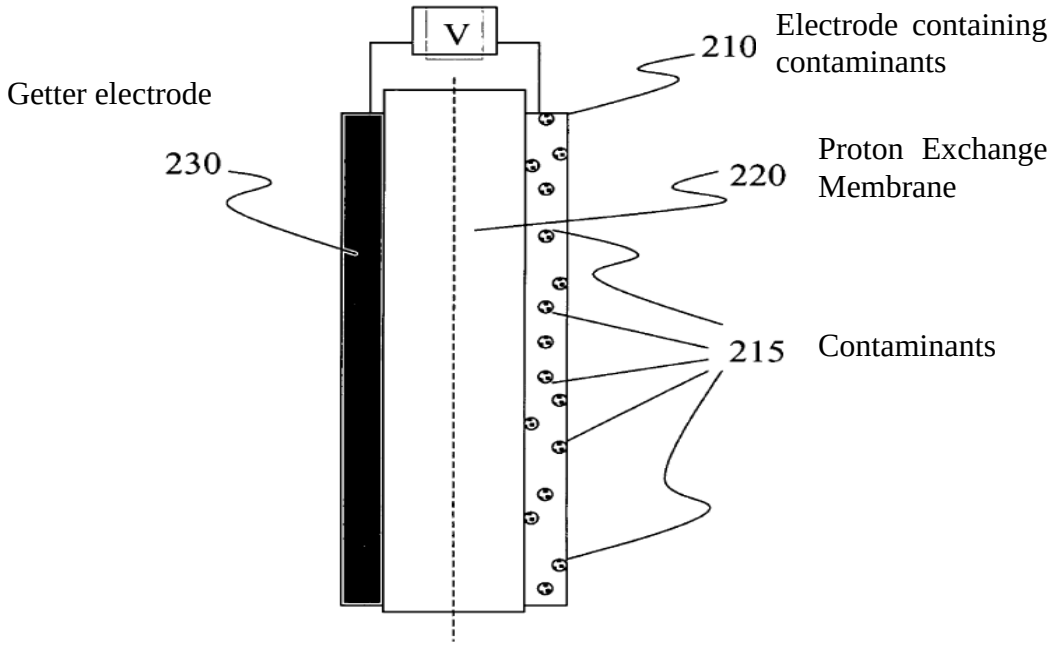

Figure 35. Schematic diagram of ruthenium contamination removal by applying a getter electrode substituted subsequently with a platinum cathode electrode [25].

As shown in Figure 35, the invention consists of an electrode (210) containing dispersed contaminants (215) on one membrane (220), and "the getter" electrode (230) which is disposed on the other membrane. The electrodes are electrically connected to provide sufficiently high potential difference to drive the contaminants from the contaminated electrode to the getter electrode. This "getter" electrode, now containing contaminants, is not of interest for further use in a fuel cell, and must be either disposed or recycled. It is then replaced with an uncontaminated electrode. If the MEA consists of one membrane instead of two thinner membranes, "the getter" electrode shall be dispersed on a GDL. The invention can be used in order to remove contaminants from the anode or the cathode. It can be applied to fuel cells operating on methanol or hydrogen reformate. It is not limited to fuel cells operating with platinum-ruthenium catalyst but also with other potentially unstable metal catalysts.

It was proven that the use of a removable "getter" electrode leads to decreased contamination and thus smaller performance loss as confirmed in [25] with CO stripping voltammetry experiments and life test experiment performed for a fuel cell with a PtRu anode catalyst and a Pt cathode catalyst.

Quantification of performance improvement due to the use of a ruthenium-depleted anode in comparison to a standard PtRu anode was carried out at Los Alamos. The anode catalyst used was PtRu black JM HiSPEC 6000 at a loading of 8 mg/cm^2, and the cathode catalyst used was Pt black JM HiSPEC 1000 at a loading of 6 mg/cm^2 The results of a 115 h life-test at 0.5 V at a cell temperature of 80^{o}C with 0.5 M methanol are shown in Figure 36.

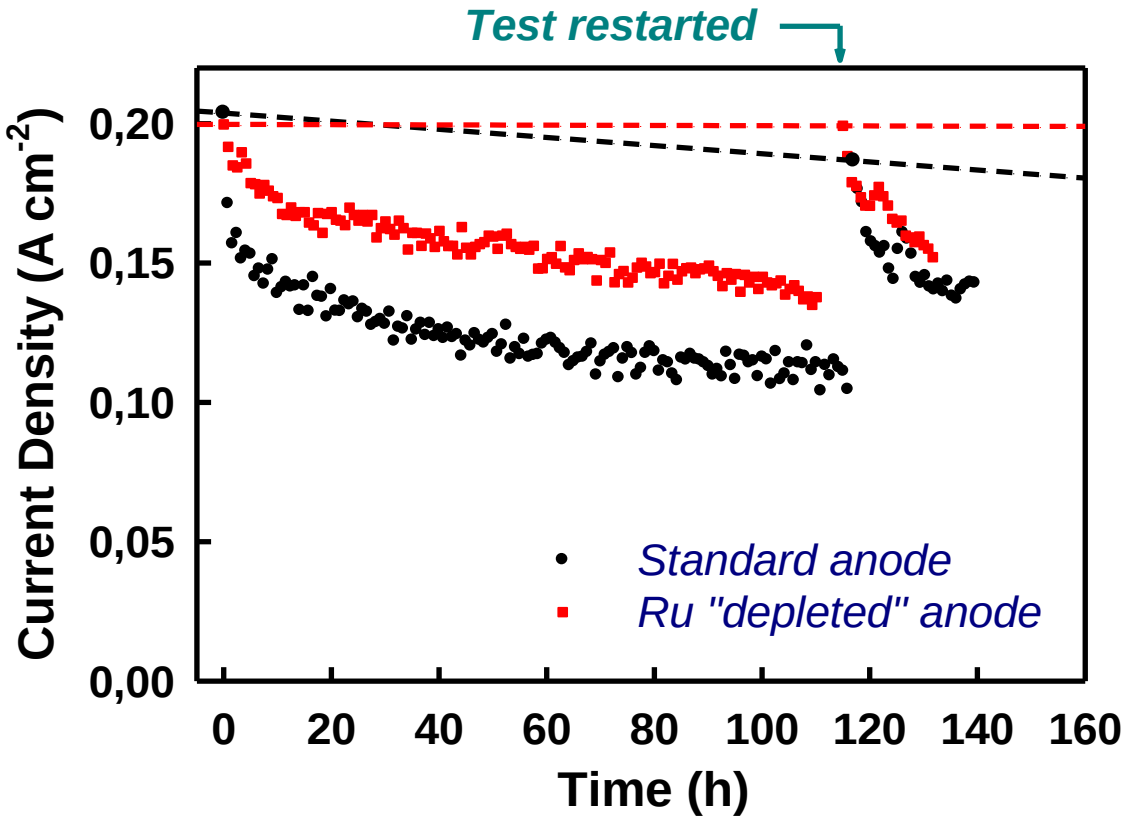

Figure 36. 115-hour DMFC life-test MEA with Ru-depleted anode (red) and with a standard PtRu anode (black) [13].

As shown in Figure 36, ruthenium-depleted anode shows no unrecoverable performance loss after 115 h of life-test, compared to 17 mA/cm^2 for standard PtRu anode. A recoverable performance loss with Ru-depleted anode is 41 mA/cm^2, compared to 73 mA/cm^2 obtained with a standard PtRu anode catalyst.

The use of Ru-depleted anode turned out to be beneficial also in terms of long-term performance loss caused by the ruthenium contamination of the cathode. After 2500 h life-time test, the unrecoverable performance loss was approximately 10 mA/cm^2, compared to 90 mA/cm^2 after a 500 h life-test in the case of standard PtRu anode catalyst.

The second path of solving the ruthenium contamination problem is finding alternative catalysts. Recently, attention was focused on developing non-precious metal cathode catalysts which would selectively reduce oxygen and not oxidize methanol. Additional requirements for the cathode catalyst are high activity towards oxygen reduction and good stability.

The main groups of compounds which seem the most promising in fulfilling those requirements are inorganic oxides, metal selenides, and pyrolyzed N_4-transition metal macrocycles and N_4-metal chelates of Fe or Co. None of those materials were reported to successfully outperform platinum catalyst in ORR activity, however, some of them show higher methanol tolerance, as reported in [26] for CoTMPP.

12 CONCLUSIONS

The complex and detailed electrochemical testing performed on DMFC MEAs with a PtRu black anode and a Pt black cathode provided detailed information on anodic and cathodic catalyst behavior, with special focus on the influence of ruthenium crossover on the oxygen reduction. All Ru-contamination processes in this work were carefully controlled and quantified, including the case of a severe cathode contamination after prolonged DMFC testing.

The initial analysis indicates that trace amounts of ruthenium can be found immediately after the MEA preparation. The contamination continues when the MEA is maintained under the OCV under humidified hydrogen-air flow. Such a current-less contamination reaches saturation after two hours. This effect is accompanied by a continuous decrease in the catalyst surface area.

Majority of the ruthenium contamination, most important from the point of view practical DMFC system, occurs during fuel cell operation, when current is passed through the cell. In order to accelerate the contamination occurring under normal operating conditions, the ruthenium containing anode was exposed to high potentials, up to 1.3 V vs. DHE. It was found that starting at an anode potential of 0.9 V, the contamination was accelerated with increasing anode potential, ultimately leading to severe cathode contamination. The overall negative shift in the CO stripping peak potential is *ca.* 230 mV. XRF data reveal a 3 wt% content of Ru in the cathode catalyst at that point. The fuel cell performance loss was determined on the basis of polarization curves. At 0.5 V the current density decreased by 66% relative to the initial performance. The cathode performance loss in the kinetic region was 80 mV and 120 mV in the mass-transport controlled region of cell operation. Anode activity for methanol oxidation was only slightly affected.

The changes in the kinetics of oxygen reduction caused by Ru contamination were quantified using of a Pt rotating disc electrode onto which ruthenium was spontaneously deposited. Subsequent spontaneous depositions resulted in a similar Ru contamination effects as those found the fuel cell experiments. Saturation Ru coverage was not achieved in the spontaneous deposition experiments probably due to insufficient deposition time. Ruthenium coverage was assessed be in the range of 0.2-0.3 ML in these experiments. The ORR half-wave potential measured at severely-contaminated Pt disk electrode was shifted negatively by 65 mV. The ORR Tafel slope increased by *ca.* 42 mV/dec in the kinetic range (0.01-0.1 mA/cm^2).

The performance degradation resulting from ruthenium crossover is unacceptably high, making it one of the main barriers against commercialization of DMFC's. At present, no alternative catalysts, either for the anode or the cathode can outperform platinum-ruthenium alloy in the oxidation of methanol (or in reformate oxidation) and platinum in oxygen reduction. The most effective method of Ru crossover mitigation developed to date involves initial anode "cleaning", which decreases the rate of Ru migration improves DMFC life-time.

The most effective method of Ru crossover mitigation developed to date involves initial anode “cleaning”, which decreases the rate of Ru migration and thus improves DMFC‟s life-time. However, further research is ongoing on alternative catalysts and improved design in order to develop a more effective solution to DMFC‟s durability problem. This research will contribute to implementing the methanol based fuel cell technology worldwide. DMFCs could possibly be of interest of Poland, as this country has great potential for low-cost methanol production.

References

1. Kamarudin, S.K., F. Achmad, and W.R.W. Daud, *Overview on the application of direct methanol fuel cell (DMFC) for portable electronic devices.* International Journal of Hydrogen Energy, 2009. **34**(16): p. 6902-6916.
2. V. Roan, D.B., A. Twining, K. Dinh, P. Wassink, T. Simmons, *AN INVESTIGATION OF THE FEASIBILITY OF COAL-BASED METHANOL FOR APPLICATION IN TRANSPORTATION FUEL CELL SYSTEMS.* University of Florida Gainesville, 2004.
3. Agency, U.S.E.P., *Clean alternative fuels: Methanol.* EPA420-F-00-040, 2002.
4. *http://forsal.pl/artykuly/383072,polska_uniezalezni_sie_od_importu_metanolu.html*.
5. Zhao, T.S., et al., *Mass transport phenomena in direct methanol fuel cells.* Progress in Energy and Combustion Science, 2009. **35**(3): p. 275-292.
6. Bagotsky, V.S., ed. *Fuel Cells Problems and Solutions*. ed. T.E. Society. 2009.
7. H. A. Gasteiger, N.M., F. N. Ross. Jr., E. J. Cairns, *CO electrooxidation on Well-Characterized Pt-Ru Alloys.* J. Phys. Chem, 1994. **98**: p. 617-625.
8. Sharon C. Thomas, X.R., Shimshon Gottesfeld, Piotr Zelenay, *Direct methanol fuel cells: progress in cell performance and cathode research* Electrochimica Acta, 2002. **47**(22-23): p. 3741-3748.
9. Liu, F., G. Lu, and C.-Y. Wang, *Low Crossover of Methanol and Water Through Thin Membranes in Direct Methanol Fuel Cells.* Journal of The Electrochemical Society, 2006. **153**(3): p. A543.
10. F.N. Buchi, M.I., T.J. Schmidt, ed. *Polymer Electrolyte Fuel Cell Durability*. ed. Springer. 2009.
11. Piela, P., et al., *Ruthenium Crossover in Direct Methanol Fuel Cell with Pt-Ru Black Anode.* Journal of The Electrochemical Society, 2004. **151**(12): p. A2053.
12. Ioroi, T., et al., *Comparative study of carbon-supported Pt/Mo-oxide and PtRu for use as CO-tolerant anode catalysts.* Electrochimica Acta, 2006. **52**(2): p. 491-498.
13. Y. S. Kim, P.Z., P. He, T. T. H. Cheng, R. Bashyam, A. P. Young, and S. Knights, *Catalyst Crossover in Polymer Electrolyte Fuel Cells*, in *4th Santa Fe Workshop on Materials and Energy Conversion*. 2010: Santa Fe.
14. X. Ren, P.Z., S. Thomas, J. Davey, S. Gottesfeld, *Recent advances in direct methanol fuel cells at Los Alamos National Laboratory.* Journal of Power Sources, 2000. **86**: p. 111-116.
15. Vidakovic, T., M. Christov, and K. Sundmacher, *The use of CO stripping for in situ fuel cell catalyst characterization.* Electrochimica Acta, 2007. **52**(18): p. 5606-5613.
16. Cuesta A, C.A., Rincon A, Perez MC, Lopez-Cudero A, Gutierrez C *Potential dependence of the saturation CO coverage of Pt electrodes: The origin of the pre-peak in CO-stripping voltammograms. Part 3: Pt(poly)* JOURNAL OF ELECTROANALYTICAL CHEMISTRY 2006. **586**(2): p. 184-195.

17. Spendelow, J.S., et al., *Electrooxidation of adsorbed CO on Pt(111) and Pt(111)/Ru in alkaline media and comparison with results from acidic media.* Journal of Electroanalytical Chemistry, 2004. **568**: p. 215-224.

18. Allen J. Bard, L.R.F., ed. *Electrochemical Methods, Fundamentals and Applications*. 2000.

19. C. L. Green, A.K., *Determination of the Platinum and Ruthenium Surface Areas in Platinum-Ruthenium Electrocatalysts by Underpotential Deposition of Copper. 2. Effect of Surface Composition on Activity.* J. Phys. Chem, 2002. **106**: p. 11446-11456.

20. Mustain, W. and J. Prakash, *Kinetics and mechanism for the oxygen reduction reaction on polycrystalline cobalt–palladium electrocatalysts in acid media.* Journal of Power Sources, 2007. **170**(1): p. 28-37.

21. Olivier Antoine, Y.B., Robert Durand, *Oxygen Reduction reaction kinetics and mechanism on platinum nanoparticles inside Nafion.* Journal of Electrochemical Society, 2001. **499**: p. 85-89.

22. van der Vliet, D., et al., *On the importance of correcting for the uncompensated Ohmic resistance in model experiments of the Oxygen Reduction Reaction.* Journal of Electroanalytical Chemistry, 2010. **647**(1): p. 29-34.

23. Paulus, U.A., et al., *Oxygen reduction on high surface area Pt-based alloy catalysts in comparison to well defined smooth bulk alloy electrodes.* Electrochimica Acta, 2002. **47**(22-23): p. 3787-3798.

24. Strbac, S., et al., *In situ STM study of nanosized Ru and Os islands spontaneously deposited on Pt(111) and Au(111) electrodes.* Surface Science, 2004. **573**(1): p. 80-99.

25. Y. S. Kim, P.Z., J. H. Choi, *Method of improving fuel cell performance by removing at least one metal oxide contaminant from a fuel cell electrode*. 2009: United States.

26. Piela, B., et al., *Highly methanol-tolerant non-precious metal cathode catalysts for direct methanol fuel cell.* Electrochimica Acta, 2010. **55**(26): p. 7615-7621.

APPENDIX A

THE EFFECT OF CO ADSORPTION TIME ON CO STRIPPING VOLTAMMETRY

The influence of adsorption time on CO coverage was quantified by performing an experiment consisting of CO stripping voltammetry for adsorption time of 5 min, 10 min 20 min and 30 min. The results are shown in Figure 37.

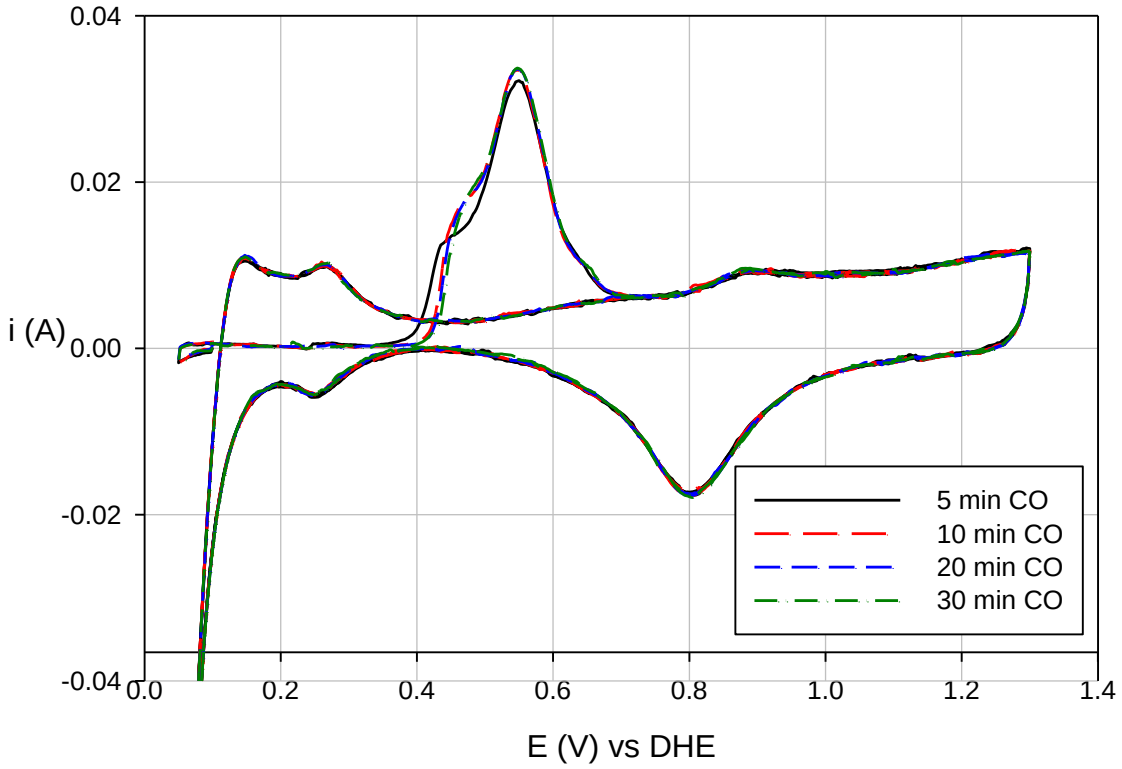

Figure 37. The influence of CO adsorption time on CO stripping voltammetry.

The voltammograms recorded after CO adsorption for 10 min, 20 min, and 30 min do not indicate any significant differences in the charge, peak potential, and shape. A slight positive shift might result from potential cycling. Based on this experiment the adsorption time in CO experiments was set to 20 minutes.

APPENDIX B

DETERMINATION OF PLATINUM RDE COLLECTION EFFICIENCY IN THE FERRICYANIDE EXPERIMENT

The experiment was performed using a three-electrode cell. The analyte solution used in the experiment was 6.4 mM potassium ferricyanide ($K_3Fe(CN)_6$) dissolved in electrolyte solution which was 1 M potassium nitrade (KNO_3) in distilled water. The working electrode was a platinum disc, the counter electrode was a platinized platinum wire, and the reference electrode was Ag|AgCl. The reference electrode was separated from the analyte solution with a frit filled with electrolyte solution in order to avoid contamination with iron.

First, the cyclic voltammetry was performed in the potential range between 0.8 V and -0.1 V vs. Ag|AgCl for scan rates of 20 mV/s, 50 mV/s, 100 mV/s, 150 mV/s and 200 mV/s. The ring potential that would ensure oxidation of the ferricyanide reduced at the disk was also determined. The results are shown in Figure 38.

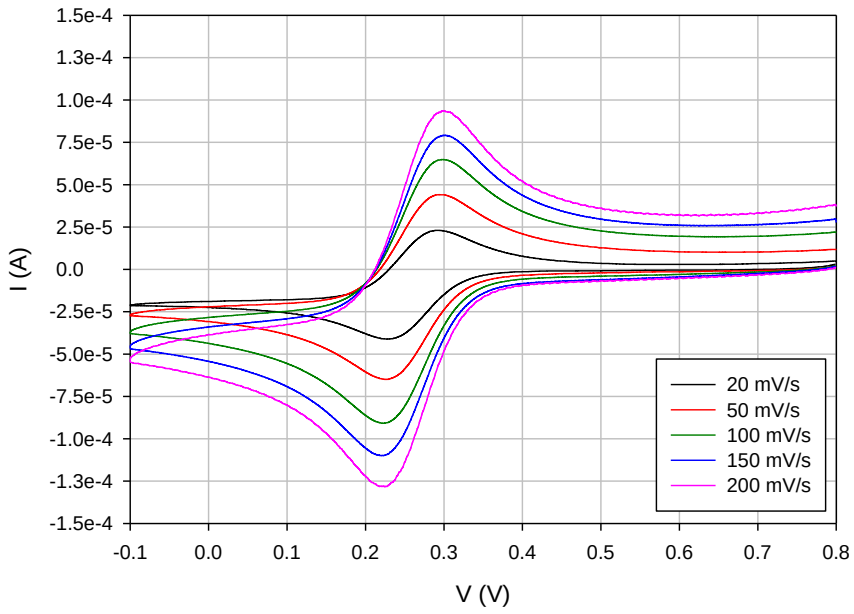

Figure 38. Cyclic voltammetry of the ferri/ferrocyanide redox couple at different rotation speeds.

The anodic and cathodic peak potentials are dependent on scan rate. For the scan rate of 200 mV/s the peak potentials are 0.24 V and 0.30 V vs. Ag|AgCl.

In order to determine the ring collection efficiency, the RRDE experiment was performed. The disc potential was swept from 0.8 V to -0.1 V vs. Ag|AgCl which caused a reduction of ferricyanide anion containing an iron atom in Fe^{3+} oxidation state to Fe^{2+}. The ring potential was kept constant at 0.6 V vs. Ag|AgCl, which caused re-oxidation of the

ferrocyanide back to ferricyanide. The collection efficiency was determined as a ratio of the current recorded at the Pt ring to the current recorded at the Pt disc. The results of the RRDE experiment are shown in Figure 39. The calculated collection efficiency was on average 23.5%.

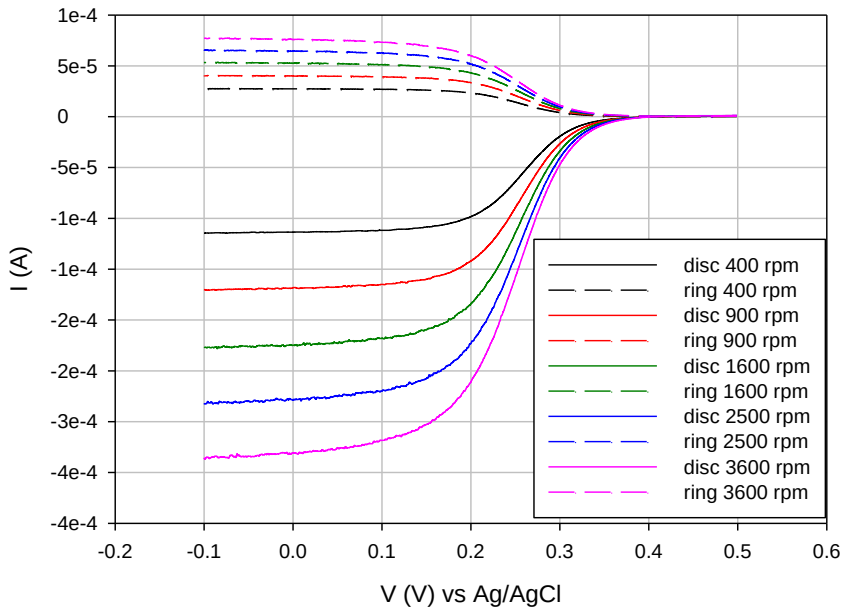

Figure 39. RRDE experiment for determining collection efficiency of platinum disc.